Professur für
Thermofluiddynamik

BACHELOR

Simulation of Self Sustained Thermoacoustic Oscillations by Coupling of a Low-Order Acoustic Network Model with a Level-Set Solver

Author:
Markus Brandl

Matrikel-Nr:
0364 2037

Supervisor:
Prof. Wolfgang Polifke, Ph. D.
Dipl.-Ing. Thomas Steinbacher

September 28, 2016

Professur für Thermofluiddynamik
Prof. Wolfgang Polifke, Ph. D.

Erklärung

Hiermit versichere ich, die vorliegende Arbeit selbstständig verfasst zu haben. Ich habe keine anderen Quellen und Hilfsmittel als die angegebenen verwendet.

Ort, Datum	Markus Brandl

Abstract

Thermoacoustic oscillations can happen in nearly every device which includes a combustion process. The reason therefore is that the combustion and the acoustics of the system interact. This leads to a coupled so-called thermoacoustic system which can either be stable or unstable. A stable system dampens out small perturbations. The other possibility is that the system gets unstable and starts to oscillate. At higher sound pressure levels this can lead to a failure of the system. In order to describe thermoacoustic systems with a laminar premixed flame the Level-Set method is used, coupled with a low-order network model. This combination enables to simulate thermoacoustic oscillations with lower computational effort than a standard Computational Fluids Dynamics (CFD) simulation would need. Furthermore, such a simplistic setup allows to carry out some very fundamental investigations where all system parameters are known. First the Level-Set solver was verified, by comparing the flame contours at different angles of a forcing cycle and by computing the Flame-Describing-Function (FDF). The results of the flame contour were as expected but the FDF showed an atypical phase behaviour. Then two different thermoacoustic coupled systems from literature were recalculated. One of them has a conical flame, the other a slit flame type. Both systems have a geometric bifurcation parameter which was used to vary the acoustics of the systems. The results were analysed with bifurcation plots and phase portraits. At several configurations a limit cycle behaviour was found for both systems.

Contents

Nomenclature

Roman Symbols

Δt	Time Step	[t]
Δx	Space Step	[m]
$\dot{Q}$	Heat Release	[W]
$\vec{x}$	Space Vector $[x, y, z]^T$	[m]
A	Flame Surface	[m^2]
A_s	System Matrix of a State-Space System	
A_t	Cross-Sectional Area of a Tube	[m^2]
B_s	Control Matrix of a State-Space System	
c	Speed of Sound	[m/s]
c_p	Specific Heat Capacity at Constant Pressure	[J/kgK]
C_s	Observer Matrix of a State-Space System	
c_v	Specific Heat Capacity at Constant Volume	[J/kgK]
CFL	Courant Friedrichs Lewy Number	[-]
D	Larger Diameter of a System	[m]
d	Smaller Diameter of a System	[m]
D_s	Straight-Way Matrix of a State-Space System	
E	Expansion Ratio	[-]
f	Frequency	[1/s]
f_{exc}	Forcing Frequency	[1/s]

f_R	Riemann Invariant	[-]
G	G-Field	
g_R	Riemann Invariant	[-]
j	Imaginary Unit	[-]
K	Phase Speed of Velocity Perturbations	[-]
L	System Length	[m]
L_f	Flame Length	[m]
Ma	Mach Number	[-]
p	Pressure	[N/m^2]
R	Ideal Gas Constant	[J/kgK]
r	Reflection Coefficient	[-]
r_f	Flame Radius	[m]
s	Laplace Variable	[1/s]
s_L	Laminar Flame Velocity	[m/s]
St	Strouhal Number	[-]
T	Temperature	[K]
t	Time	[s]
t_{on}	Start Time for Velocity Field	[s]
u	Velocity Component in x-Direction	[m/s]
u_{conv}	Convective Velocity	[m/s]
v	Velocity Component in y-Direction	[m/s]
x	Space Coordinate	[m]
x_s	Bifurcation Parameter	[m]
y	Space Coordinate	[m]

Functions

$\phi(\cdot)$	Phase of a Transfer Function

$\Psi(\cdot)$	Function in Hamilton-Jacobi Equation
$\sigma_H(\cdot)$	Heaviside Function
$G(\cdot)$	Gain of a Transfer Function
$G_t(s)$	Transfer Function in the Frequency Domain
$H(\cdot)$	Function in Hamilton-Jacobi Equation
$L(u)$	Vector Function
$TV(\cdot)$	Total Variation
$u_s(t)$	Input Vector for a State-Space System
$X(s)$	Input Signal in the Frequency Domain
$x_s(t)$	State-Space Vector of a State-Space System
$Y(s)$	Output Signal in the Frequency Domain
$y_s(t)$	Output Vector for a State-Space System

Greek Symbols

β_f	Flame Aspect Ratio	[-]
ϵ	Normed Velocity Perturbation Amplitude	[-]
γ	Heat Capacity Ratio	[-]
ω	Angular Frequency	[1/s]
ω_{exc}	Forcing Angular Frequency	[1/s]
Φ	Equivalence Ratio	[-]
ρ	Density	[kg/m^3]
σ	Growth Rate	[1/s]
τ	Period Time	[s]
θ	Temperature Excess	[-]

Modifiers and mathematical operators

$(\cdot)_{ref}$	Value at Reference Point
$(\cdot)^*$	Normed Signal Fluctuation

$(\cdot)^T$	Transpose of a Matrix
$(\cdot)_c$	Value before a Flame Element
$(\cdot)_d$	Downstream Parameter
$(\cdot)_h$	Value after a Flame Element
$(\cdot)_n$	Normal Component
$(\cdot)_R$	Riemann Invariant
$(\cdot)_t$	Tangential Component
$(\cdot)_u$	Upstream Parameter
$\bar{(\cdot)}$	Mean Value
$\nabla(\cdot)$	Gradient
$\frac{\partial^2}{\partial a^2}(\cdot)$	Second Partial Derivation
$\frac{\partial}{\partial a}(\cdot)$	First Partial Derivation
$\oint(\cdot)da$	Line Integral

Acronyms

1D	One Dimensional
2D	Two Dimensional
3D	Three Dimensional
CFD	Computational Fluid Dynamics
ENO	Essentially Non Oscillatory Discretization Scheme
FDF	Flame-Describing-Function
FFT	Fast Fourier Transformation
FTF	Flame-Transfer-Function
GFcase	Data Structure for GFlame
GFlame	Level-Set Solver
LTI	Linear Time Invariant System
MIMO	Multiple Input Multiple Output System

ODE	Ordinary Differential Equation
PDE	Partial Differential Equation
SISO	Single Input Single Output System
taX	Acoustics Program
TVD	Total Variation Diminishing Scheme
WENO	Weighted Essentially Non Oscillatory Discretization Scheme

1 Introduction

In the last century more powerful engines for rockets and jet-powered aircrafts were developed than in the centuries before. These engines have a higher power density than anything before. The energy is introduced to the system by chemical combustion. Such a combustion process is so complex that it is hard to describe it with each aspect. So, for many rocket engines the combustion got unstable and the flame started to oscillate. This mostly caused a complete failure of the system which was destroyed by the high pressure waves. The engineers found out that these instabilities happened by thermoacoustic interactions which means that the flame and the acoustics of the system interact. Under certain conditions this can lead to thermoacoustic oscillations which can damage the system.

These interactions are very complex because there are many factors which influence such a thermoacoustic system. As described by Polifke (2004) it is not a local phenomena. The whole system must be considered which makes the problem so complicated. To simplify the problem only the acoustics and the combustion are considered. Under certain conditions a system modelled by just these two elements can start to oscillate. With the linear control theory it is not possible to predict the amplitude of such a thermoacoustic oscillation. Therefore the non-linearity has to be considered. According to Sujith et al. (2016) in rocket engines the acoustics have to be treated non-linear but the combustion can be considered as a linear phenomena. If the power density is reduced as in burners or gas turbines, the behaviour changes. In such systems the non-linearity of the combustion is important and the acoustics can be treated linear. This is caused by the smaller pressure during the combustion process. For gas turbines it is important to analyse the thermoacoustic stability, because an unstable system can get damaged. The damage here is not caused by the pressure waves but by hotter regions inside the combustion.

The main problem of the prediction of thermoacoustic oscillations are the computational models. To simulate such oscillations in most cases a Computational Fluid Dynamics (CFD) simulation is needed, which includes a combustion model. The computational time can be reduced if some assumptions are made. In this thesis the following simplifications were made to describe the thermoacoustic behaviour of a system as for example a burner:

- Small mean flow velocities and low Mach numbers
- Linearised acoustics due to small pressure perturbations
- Premixed burnable gas
- Laminar combustion

The linearised acoustics are described by using a low-order network model. Such a model is used to simulate the acoustics in one dimension (1D) of a thermoacoustic system. The flame is a laminar premixed flame which is described with a Level-Set approach. With such a method the behaviour of a flame can be computed with much less computational effort than a CFD simulation. Thus it is possible to simulate thermoacoustic systems much faster.

The main target of this thesis is to simulate the thermoacoustic behaviour of unstable systems which start to oscillate. The oscillations are only caused by the system itself and have no external excitement. Thermoacoustic systems were analysed for their amplitudes and also their oscillation types. The target was to find a limit cycle oscillation which is an oscillation that repeats every cycle.

2 Theoretical Fundamentals

For a thermoacoustic coupled simulation it is necessary to combine the properties of a heat source and an acoustic model. In this thesis the acoustics are covered by a linearised wave model and the heat source is a non-linear flame model. The flame model needs a hydrodynamic velocity field, acting on the flame surface. After modelling the flame, the system gets analysed to verify the correct implementation. The acoustics can be coupled with the hydrodynamic velocity field which then affects the flame front. The flame front is proportional to the heat release which has an influence on the acoustics. This feedback loop can cause different types of oscillations. By considering the acoustic system without a flame and with a linear flame model it is possible to predict the non-linear results.

2.1 Flame Modelling

The Level-Set method is used in this thesis to model the non-linear flame. This model computes the non-linear heat release of a flame, depending on the inlet velocity of the unburned gas mixture. The simulation results also depend on the laminar flame velocity which can be approximated by using correlations. The laminar flame velocity vary for different fuels and oxidisers.

2.1.1 Level-Set Method

In order to model a laminar premixed flame the Level-Set method or so-called G-Equation is used. This method computes the behaviour of a function of $(n-1)$-th order in a space of n-th order with $n \in \mathbb{N}$. Therefore, the speed of the surface in dependency of the curvature of the function is used. With the Level-Set method for example crystal growth and flame propagation can be computed as described by Osher and Sethian (1988). Equation (2.1) shows the general Hamilton-Jacobi equation as proposed by Serna and Qian (2006).

$$\frac{\partial \Psi}{\partial t} + H(\vec{x}, \Psi, \bigtriangledown \Psi) = 0, \quad \Psi(\vec{x}, 0) = \Psi_0(\vec{x}), \quad \vec{x} \in \mathbb{R}^n, \quad t > 0 \tag{2.1}$$

In this equation Ψ is the searched function which depends on the space vector $\vec{x}$ and the time t. H is an arbitrary function. It can consist of the space vector, the function Ψ and the derivative of Ψ.

For this thesis a solver based on the G-Equation in two dimensions (2D) was used. It can be written as denoted in equation (2.2).

$$\frac{\partial G}{\partial t} + u\frac{\partial G}{\partial x} + v\frac{\partial G}{\partial y} = s_L\sqrt{\left(\frac{\partial G}{\partial x}\right)^2 + \left(\frac{\partial G}{\partial y}\right)^2} \tag{2.2}$$

The variable G is a scalar field which is used to construct the flame surface. It is called the G-Field. Furthermore u and v are the velocity components at every point of the G-Field. The laminar flame velocity s_L specifies the speed of the flame front perpendicular to itself. In figure 2.1 a burner is shown with a laminar flame front.

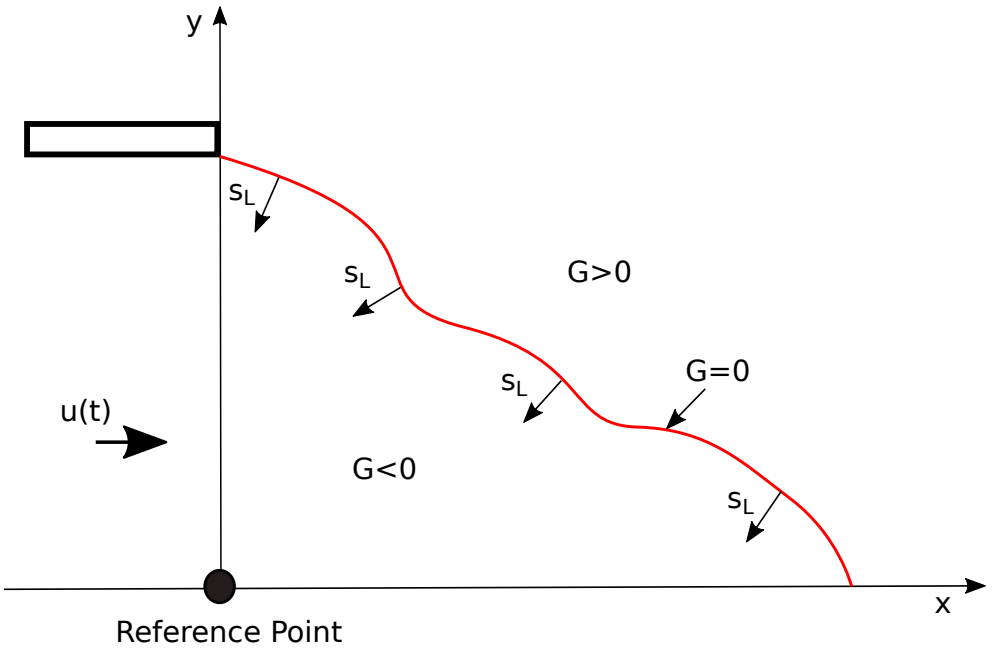

Figure 2.1: Flame front propagation of a laminar pemixed flame based on the Level-Set method.

The G-Equation describes a moving surface in a three dimensional space. To get the current flame curve the intersection of the G-Field with the zero level in the third dimension is computed. This means that the flame is modelled as a discontinuity. For every point in the G-Field with a value $G < 0$ applies that the mixture is unburned. The already burned mixture is defined by $G > 0$. The infinite small flame front is specified by $G = 0$. In dependency of the used fuel, the oxidator and their equivalence ratio, the laminar flame velocity s_L can be calculated. Therefore, different models are known. One of them is described in chapter 2.1.2. The last variables which are needed to describe the problem are u and v. They specify the velocity field of the unburned gas mixture acting on the G-Field. The velocity at the reference point is used to build up the velocity field. This operation is described in chapter 2.2.

The Level-Set method is often used to describe laminar premixed flames because it needs much less computation effort than a full computational fluid dynamics (CFD) simulation. Such a model was used for instance by Cuquel et al. (2011) and also by Schuller et al. (2003) to predict the flame front propagation. Dowling (1999) and Kashinath et al. (2013b) use the

G-Equation coupled with a very basic acoustic model to simulate limit cycles. Kashinath et al. (2014) published results which are comparable with the results gained in this thesis. Orchini et al. (2015) uses the G-Equation and also an acoustic model similar to the software setup described in chapter 3.

2.1.2 Laminar Flame Velocity

The laminar Flame velocity determines the speed of the flame front perpendicular to itself. It can be measured with a so-called 'combustion bomb'. That is basically a sphere filled with burnable gas which is ignited at the center. Then the expansion of the flame front is measured and the burning velocity can be recalculated. So the value can be fixed for a specific mixture at certain environment conditions.

In order get a more flexible method to obtain the laminar flame velocity, different theories are known to calculate it. Most of them depend on the equivalence ratio Φ of the unburned gas. This value describes the ratio between the oxidizer and the fuel. In this thesis the correlation (2.3) from Lieuwen (2003) was used if only the equivalence ratio was known.

$$s_L = C_A \cdot \Phi^{C_B} \cdot e^{-C_C} \cdot (\Phi - C_D)^2 \tag{2.3}$$

This correlation is only valid for methane/air mixtures at atmospheric pressure and $300K$ temperature. The constants which were used are listed in table 2.1. To get the laminar flame velocity for other ambient conditions, there are some correction laws (see e.g. Poinsot and Veynante (2005)).

Table 2.1: Constant values for the laminar flame velocity correlation shown in equation (2.3).

$C_A = 0.6079$	$C_B = -2.554$	$C_C = 7.31$	$C_D = 1.23$

2.2 Velocity Fields

The G-Equation needs an overlain velocity field as can be seen in equation (2.2). For that, different models are used. Some of them are very simple, some are more sophisticated. The velocity field in flow direction is depending on the reference velocity at the source (commonly at the center of the source channel). Perpendicular to the flow, the velocity field can be calculated with different models. So the reference velocity is the value which is used to couple the G-Equation solver with the environment, for example with an acoustic model as was done in this thesis. In the following sections three important models are described to generate a velocity field.

2.2.1 Uniform Velocity Model

One of the simplest velocity model is the so-called 'Uniform Velocity Model'. This model only has components in the main flow direction as denoted in equation (2.5). The magnitude of

the transient flow on every point of the vector field is the same. The velocity oscillates with a given amplitude and a given frequency around the mean flow speed. This velocity model was used by Fleifil et al. (1996). It is just a simple sine function as written in equation (2.4).

$$u(t) = \bar{u} \cdot \left(1 + \epsilon \cdot \sin(2 \cdot \pi \cdot f_{exc})\right) \tag{2.4}$$

$$v(t) = 0 \tag{2.5}$$

It can readily be seen that this equation only depends on the time variable. The variable ϵ defines the normed velocity perturbation amplitude of the system and f_{exc} is the forcing frequency. This basic variables are needed in most of the velocity models.

2.2.2 Convective Velocity Model

A much more realistic model is the 'Convective Velocity Model'. This one produces a convecting wave which travels from the flame base to the flame tip. This velocity field is defined by equation (2.6).

$$u(x,t) = \bar{u} \cdot \left(\epsilon \cdot \sin\left(2 \cdot \pi \cdot f_{exc} \cdot \left(t - \frac{x - x_{ref}}{u_c} - t_{on}\right)\right) \cdot \sigma_H(t - t_{on}) + 1\right) \tag{2.6}$$

$$v(x,t) = 0 \tag{2.7}$$

Now the velocity field also depends on the spatial variables. At each point at any time the velocity in stream direction can be determined. The velocity component perpendicular to the stream is set to zero again as written in equation (2.7). In this equation t_{on} defines the start time and x_{ref} is the position of the reference point . σ_H is a Heaviside function which is zero for $\sigma_H(t < 0)$ and one for $\sigma_H(t \geq 0)$. The velocity of the propagating wave is determined by the convective velocity u_c. This type of velocity field was first used by Schuller et al. (2003). In figure 2.2 an example for a convective velocity field can be seen.

The blue line represents the flame surface. The sine waves of the velocity field are depicted overlain by the flame surface curve.

2.2.3 Convective Incompressible Velocity Model

To get a pretty realistic velocity model the convective type is modified by using the continuous equation (2.8).

$$\frac{\partial u}{\partial x} + \frac{\partial v}{\partial y} = 0 \tag{2.8}$$

This equation ensures the mass conservation in a incompressible fluid. So the velocity components normal to the stream direction can be evaluated. The x-components are calculated as for the convective type. In y-direction the velocity can be computed by inserting equation 2.6 in equation (2.8). By solving the resulting ordinary differential equation (ODE)

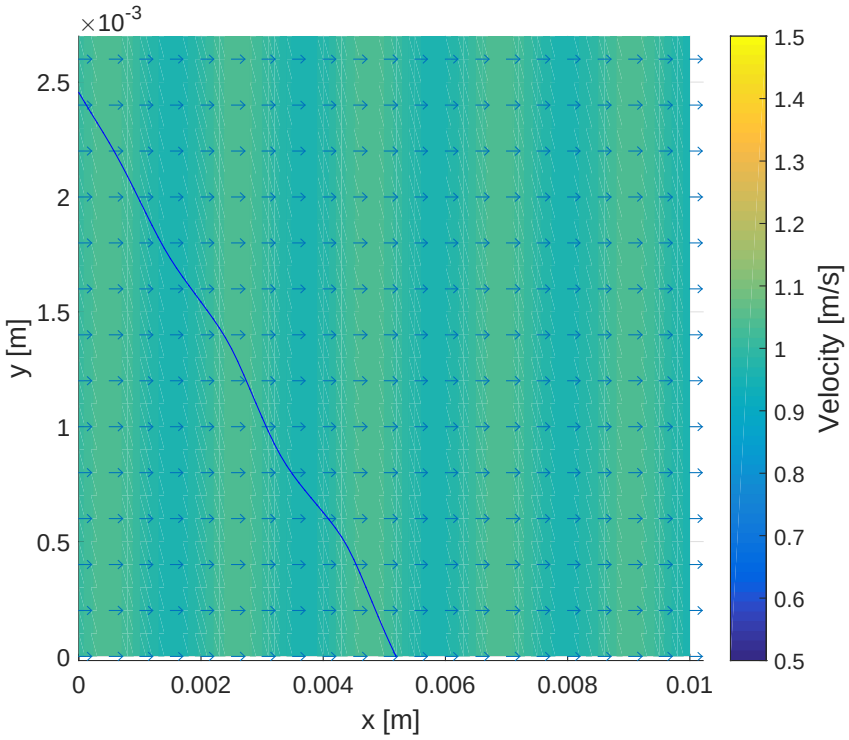

Figure 2.2: Example of a convective velocity field.

the second velocity component can be evaluated. Such a velocity field was used by Cuquel et al. (2011) and also by Kashinath et al. (2013b). The results gained by Orchini et al. (2015) are as well computed with a convective incompressible velocity model.

2.3 Acousics Modelling

The acoustics, used in this thesis, are modelled as linearised 1D equations. Complex acoustic systems can be build up by using a network model. This allows to design simple acoustic elements and connect them to a complex system. The acoustic system was used to export a State-Space system which was coupled with the Level-Set solver.

2.3.1 Low-Order Network Model

In order to build complex acoustic systems, in this thesis a software based on the so-called 'Low-Order Network Model' was used. It divides the system in many simple parts in which the acoustics can be modelled very easily. So per element there are two equations which describe the behaviour of the fluid inside. At the boundary conditions there are two more equations attached. Some of the important elements and boundary conditions are described in the next sections. After identifying all the needed equations they can be written as a system matrix. It

is possible to solve this system of equations for the so-called 'Riemann Invariants' which are described in chapter 2.3.2. These Riemann invariants can be used to reconstruct all primitive variables. With this system it is also possible to search for eigenfrequencies and to check the system for stability.

2.3.2 Duct Element

The acoustics in duct elements can be described by velocity and pressure. For small perturbations and if small energy amounts are introduced to a system, the acoustics can be used linearised and considered to be incompressible. The general form of the momentum conservation equation in x-direction for a 1D incompressible case is given in equation (2.9). It is a so-called 'Euler Equation' which means that the viscosity of the fluid is neglected.

$$\frac{\partial u}{\partial t} + u \cdot \frac{\partial u}{\partial x} = -\frac{1}{\rho} \cdot \frac{\partial p}{\partial x} \tag{2.9}$$

In this equation the density is written as ρ and also the pressure p is needed to describe the momentum conservation. The variable u is as specified before the velocity in x-direction. To simplify the model and to reduce the computational time the equation is linearised to the form of equation (2.10).

$$\frac{\partial^2 p'}{\partial x^2} - \frac{1}{c^2} \cdot \frac{\partial^2 p'}{\partial t^2} = 0 \tag{2.10}$$

$$c = \sqrt{\gamma \cdot R \cdot T} \tag{2.11}$$

In equation (2.10) the speed of sound appears as c. It can be calculated with equation (2.11). In this equation R is specified as the ideal gas constant and $\gamma = c_p / c_v$ as the heat capacity ratio. The variable c_p is the specific heat capacity at constant pressure and c_v is the specific heat capacity at constant volume. T describes the temperature of the gas. Based on this linearised equation the solution for the characteristic waves is given in equation (2.12).

$$p'(x,t) = f_R\left(t - \frac{x}{c+u}\right) + g_R\left(t + \frac{x}{c-u}\right) \tag{2.12}$$

In acoustic applications it is common to use so-called 'Riemann Invariants'. They merge the primitive variables of a system as described by the equations (2.13) and (2.14). The quotation mark at the velocity and the pressure implies that they are perturbations. They are calculated by using the equations (2.15) and (2.16).

$$f_R = \frac{1}{2} \cdot \left(\frac{p'}{\rho \cdot c} + u'\right) \tag{2.13}$$

$$g_R = \frac{1}{2} \cdot \left(\frac{p'}{\rho \cdot c} - u'\right) \tag{2.14}$$

$$u' = u - \bar{u} \tag{2.15}$$

$$p' = p - \bar{p} \tag{2.16}$$

In the equations (2.15) and (2.16) the variables u and p represent the velocity and pressure signal and $\bar{u}$ and $\bar{p}$ are their mean values. The Riemann invariants can be seen as two characteristic waves which travel through the system with the speed of sound. The f_R-wave travels downstream and the g_R-wave travels in the opposite direction upstream. A more detailed explanation was published by Polifke (2004). If this wave equations are transformed to the frequency domain as described by Emmert et al. (2014) a matrix system can be build up as in equation (2.17).

$$\begin{pmatrix} g_{R,u}(s) \\ f_{R,d}(s) \end{pmatrix} = \begin{pmatrix} 0 & e^{-\frac{l}{c-u}\cdot s} \\ e^{-\frac{l}{c+u}\cdot s} & 0 \end{pmatrix} \begin{pmatrix} f_{R,u}(s) \\ g_{R,d}(s) \end{pmatrix} \tag{2.17}$$

The matrix form represents the mathematical description of a tube element. In this case $f_{R,u}$ and $g_{R,u}$ are the Riemann invariants on the upstream side and $f_{R,d}$ and $g_{R,d}$ are located downstream. The variable l is the length of the tube segment and s is the Laplace variable defined as $s = j\omega + \sigma$. The variable ω describes the angular frequency and σ the growth rate. The imaginary unit is written as j.

These tube elements and other elements which can be described with two equations, now can be stacked to larger systems. The connection between two elements are always one f_R- and one g_R-wave. An example of the connection between several simple elements is shown in figure 2.3.

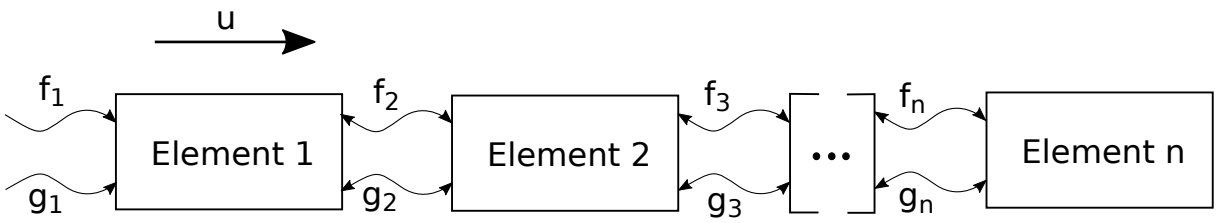

Figure 2.3: Example of connected simple elements of a low-order network model.

2.3.3 Area Jump

An area jump can be easily computed by using the continuity equation. It is assumed that the pressure over the area jump is constant. This leads to the equations (2.18) and (2.19).

$$p'_u = p'_d \tag{2.18}$$

$$A_{t,u} u'_u = A_{t,d} u'_d \tag{2.19}$$

With equation (2.19) it is possible to calculate the velocity change over the area jump. In this formula $A_{t,d}$ is the downstream cross-sectional area of the tube and $A_{t,u}$ the upstream one. The pressure fluctuation is not affected as can be seen in equation (2.18).

2.3.4 Flame Element

There are several simplifications by modelling the flame element in a low-order network model. The pressure change over the flame element can be neglected and the velocity increases due to the heating of the fluid. Based on mass conservation the velocity increases with an increasing temperature. One simple approach is the '$n-\tau$-model'. This model is basically a time lag between the input velocity perturbation and the resulting heat release change (see e.g. Polifke (2004)).

The flame model in the low-order network model affects the acoustics of the whole system. There are the so-called 'Rankine-Hugoniot-Equations' which can be used to describe the flame. This set of equations is linearised as each element in the acoustic model used here. The linearised forms are written in equation (2.20) and in equation (2.21). The derivation of these equations can be found in Kopitz and Polifke (2008).

$$p'_d = p'_u - \rho_c \cdot u_c^2 \cdot \theta \cdot \left(\frac{u'_u}{u_c} + \frac{\dot{Q}'}{\bar{\dot{Q}}} \right) \tag{2.20}$$

$$u'_d = u'_u + u_c \cdot \theta \cdot \left(\frac{\dot{Q}'}{\bar{\dot{Q}}} - \frac{p'_u}{p_c} \right) \tag{2.21}$$

These equations describe the change of the pressure fluctuation and the velocity fluctuation over a flame element in the acoustic system. The variables ρ_c and u_c describe the density and the velocity of the fluid upstream on the cold side of the flame. $\dot{Q}'$ is the heat release fluctuation of the flame which depends on the flame surface. The mean value of the heat release is written as $\bar{\dot{Q}}$. The variable θ specifies the temperature excess which is denoted in equation (2.22).

$$\theta = \left(\frac{\bar{T}_h}{\bar{T}_c} - 1 \right) \tag{2.22}$$

Here $\bar{T}_c$ specifies the mean value of the temperature before the flame element and $\bar{T}_h$ is the mean temperature after the combustion. Note that in this acoustic model for a flame element the dimensions of the flame are neglected which means that it is acoustically compact.

2.3.5 Boundaries

In order to describe the acoustic behaviour at the ends, a coefficient called reflection coefficient r is introduced. It is defined as the ratio between the Riemann invariants at the boundary. In equation (2.23) the definition for the inlet is shown.

$$r = \frac{g_R}{f_R} \tag{2.23}$$

If the equations (2.13) and (2.14) are inserted and then the equations are simplified this leads to the values for the primitive variables u' and p'. The reflection coefficient can vary

between -1 and 1. For closed ends applies $r = 1$ which means that $u' = 0$. $r = -1$ applies for open ends and therefore $p' = 0$. If the value for open ends is a little bit higher than -1 it is meant to cover losses at an outlet of a system. Note that these values are very important for the linear stability of a system.

2.3.6 State-Space Systems

In the time domain a common approach to describe a 'Linear Time-Invariant System' (LTI-System) is a State-Space system. It is used to export the acoustics as a 'Single-Input-Single-Output' system (SISO). Such a system can be loaded by the Level-Set solver to cover the acoustic effects. A State-Space system is a combination of a linear ODE and a linear equation. The system can be written as equations (2.24) and (2.25).

$$\frac{\mathrm{d}}{\mathrm{d}t} x_s(t) = A_s \cdot x_s(t) + B_s \cdot u_s(t), \;\; x_s(0) = x_{s,0} \tag{2.24}$$

$$y_s(t) = C_s \cdot x_s(t) + D_s \cdot u_s(t) \tag{2.25}$$

This system has an input vector $u_s(t)$ and an output vector $y_s(t)$. The variable $x_s(t)$ is the State-Space vector. The other variables are listed in table 2.2.

Table 2.2: Matrices used by a State-Space model.

Variable	Description
A_s	System Matrix
B_s	Control Matrix
C_s	Observer Matrix
D_s	Straight-Way Matrix

First the ODE is solved to get the State-Space vector, then this vector and the input vector are used to calculate the output vector by using the linear equation. A further description can be found in Lunze (1996).

2.4 Flame Identification

Flames can be described with different models. Therefore it is important to specify the transmission behaviour of a flame. Linear flame models can be described easily by the Flame-Transfer-Function. More difficult is the transmission behaviour of a non-linear flame. One approach is to modify the Flame-Transfer-Function to the Flame-Describing-Function. In order to identify such transfer functions a Sine-Sweep method can be used.

2.4.1 Linear Flame-Transfer-Function

In order to describe linear system behaviour, the linear control theory provides the concept of the so-called transfer functions. As shown in equation (2.26) the function depends on a complex variable and defines the relation between the input signal $X(s)$ and the output signal $Y(s)$ (see e.g. Lunze (1996)). This method can also be used to describe the behaviour of a flame.

$$G_t(s) = \frac{Y(s)}{X(s)} \tag{2.26}$$

For a flame the relation between the velocity fluctuation at the reference point and the heat release fluctuation is of interest. To get more standardised functions for the transfer behaviour the input and output signals are normed with their mean values. This leads to the Flame-Transfer-Function (FTF) in equation (2.27) (see e.g. Noiray et al. (2008)).

$$FTF = \frac{\dot{Q}'/\bar{\dot{Q}}}{u'/\bar{u}} \tag{2.27}$$

For laminar premixed flames with a constant density the normed heat release fluctuation can be replaced by the normed surface fluctuation (see e.g. Lieuwen (2003)). This simplifies the computation of the FTF. Thus the transfer function is defined as in equation (2.28).

$$FTF = \frac{A'/\bar{A}}{u'/\bar{u}} \tag{2.28}$$

It is important to know that the FTF covers only linear effects. The reason for that is, as described by Noiray et al. (2008), that the FTF is only depending on the frequency of the velocity fluctuation. For visualization the transfer function can be written as in equation (2.29) and the gain and phase can be plotted as a bode diagram to show the transfer behaviour. The gain G can be described as the amplifying effect of the transfer function on the input signal. The phase ϕ specifies the shift of the phase between the input signal and the output signal (see e.g. Lunze (1996)). Both parameters are only depending on the forcing angular frequency ω_{exc}.

$$FTF = G(\omega_{exc}) \cdot e^{j \cdot \phi(\omega_{exc})} \tag{2.29}$$

An example of a FTF is plotted in figure 5.6. In this figure the FTF for a conical flame is shown. Instead of the forcing angular frequency ω_{exc} the forcing frequency f_{exc} is used. It is defined as $f_{exc} = \frac{\omega_{exc}}{2 \cdot \pi}$. It can be seen that the gain is decreasing with an increasing forcing frequency f_{exc}. This shows the low-pass filter behaviour of a flame. Also the phase decreases nearly linear with an increasing f_{exc} which is also characteristic for a low-pass filter. This means that the signal shift increases.

2.4.2 Non-Linear Flame-Describing-Function

In order to get a limit cycle it is necessary to get a non-linear element in the system. As the acoustics are linearised, the flame is the non-linear part. The G-Equation provides such a non-linear behaviour. That cannot be gained by using an analytical solution. Further informations are in Noiray et al. (2008).

It is important to analyse the transfer behaviour of a non-linear flame. One approach to get a proper description is to use a Flame-Describing-Function (FDF). It is basically a set of different transfer functions. Now the transfer function is depending on the frequency as the FTF but also on the forcing amplitude of the velocity fluctuation. This means that the transfer function depends on the input variable which leads to the non-linear behaviour. It is also assumed that the oscillations are harmonic and the frequency from input to output does not change. The transfer function can be written as in equation (2.30).

$$FDF(\omega_{exc}, \left|u'\right|) = \frac{A'/\bar{A}}{u'/\bar{u}} = G(\omega_{exc}, \left|u'\right|) \cdot e^{i \cdot \phi(\omega_{exc}, \left|u'\right|)} \tag{2.30}$$

For the visualisation of such a Flame-Describing-Function also bode plots can be used. These graphs are plotted similar to a FTF gain and phase plot. They are plotted over the forcing angular frequency but now there are more curves for different forcing amplitudes. Such graphs are used in chapter 4.

2.4.3 Sine-Sweep Identification Approach

A non-linear Flame-Describing-Function can be computed with the Sine-Sweep method. This identification method can calculate the transfer function for one specific forcing amplitude. In chapter 4 this identification was done at different forcing amplitudes and afterwards the results were merged to the FDF.

The method discretizes the observed frequency range in certain frequencies. Then a sine signal is generated for each frequency at a specific amplitude and with a predefined number of periods. Now all sine signals are merged to one signal with increasing frequency. Such a signal is shown in figure 2.4. It shows 30 frequencies between $0Hz$ and $300Hz$ with each 3 periods long.

This signal is now used as the reference velocity for a velocity field which is generated as described in chapter 2.2. Now by solving the G-Equation, the flame surface signal A can be computed. The input signal u and the output signal A were normed by using their mean values as shown in equations (2.31) and (2.32). These standardisation of values is indicated by $(\cdot)^*$ and is later done for other values too. Next both normed signals were merged as described by equation (2.30).

$$u(t)^* = \frac{u(t) - \bar{u}}{\bar{u}} = \frac{u'}{\bar{u}} \tag{2.31}$$

$$A(t)^* = \frac{A(t) - \bar{A}}{\bar{A}} = \frac{A'}{\bar{A}} \tag{2.32}$$

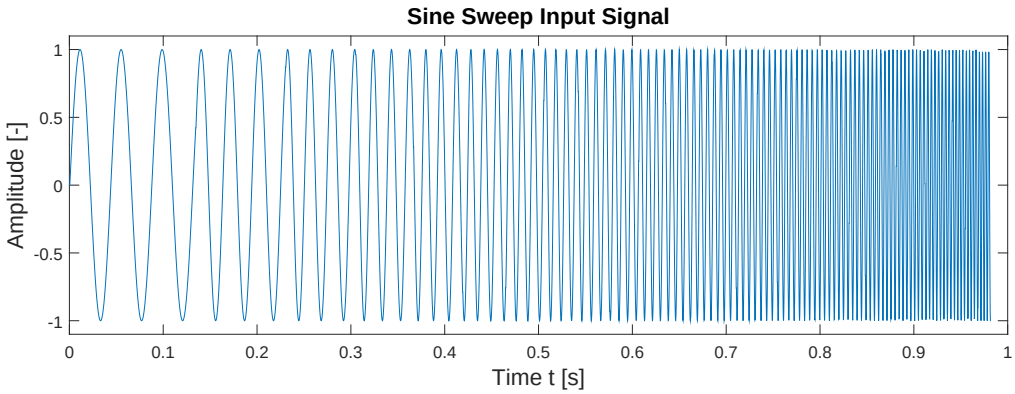

Figure 2.4: Intput signal for a Sine-Sweep identification.

2.5 Limit Cycles

A thermoacoustic system consisting of a heat source and an acoustic model can start to oscillate under certain conditions. One way to describe such conditions is the Rayleigh Criterion which is defined as the relation between pressure and heat release. If a system starts to oscillate, there are different types of oscillation. By using Fast-Fourier-Transform methods and phase portraits these oscillations can be analysed.

2.5.1 Limit Cycle Fundamentals

In a thermoacoustic system like a burner or a jet engine the system acoustics and the combustion interact. Depending on the Rayleigh criterion described in 2.5.2 this can cause a stabilizing or destabilizing behaviour of the system. In this thesis just the increasing behaviour is considered. As explained by Dowling (1997), the linear theory only describes an exponential growth without a saturation of the system. So it is not possible to make a prediction of the amplitudes of an unstable system by only using linear methods. It is necessary to implement a non-linearity to the system to get a steady-state oscillation like a limit cycle.

Because of the low flow velocity in the considered cases, the Mach numbers in the systems are very low. Even for high perturbations it is possible to assume a linear behaviour as written by Dowling (1997). So a linear acoustic behaviour is absolutely justifiable.

This means that the non-linearity has to be in another part of the system. According to Sujith et al. (2016) there are three main sources of non-linearity. First is the acoustic sytem which is only non-linear at high Mach numbers as in rocket engines. Second is the damping of the system. Such an influence due to the flame non-linearity was used by Kashinath et al. (2013b). The third possible source of non-linearity is the heat release of the combustion. It has the strongest non-linear behaviour at the used system conditions. In fact it means that the heat release saturates, which leads to an oscillation at large amplitudes of the system. This oscillation can be a limit cycle with one or multiple frequencies, a quasi periodic oscillation or a chaotic behaviour as shown by Orchini et al. (2015). The velocity graph of one possible

oscillation is shown in figure 2.5. The different types are considered in chapter 2.5.4.

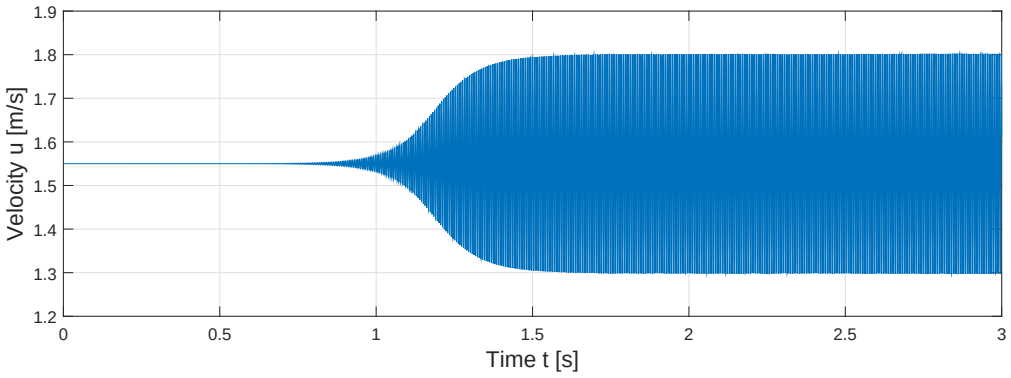

Figure 2.5: Increasing and saturation of the velocity of an unstable thermoacoustic system.

The frequency of the oscillation is commonly determined by the first mode of the acoustic system but it can shift a little bit due to the change of the acoustic behaviour with the flame model (see e.g. Emmert et al. (2016)). It is also possible that a second mode gets dominant after an oscillation has already evolved. An example is shown in figure 2.6.

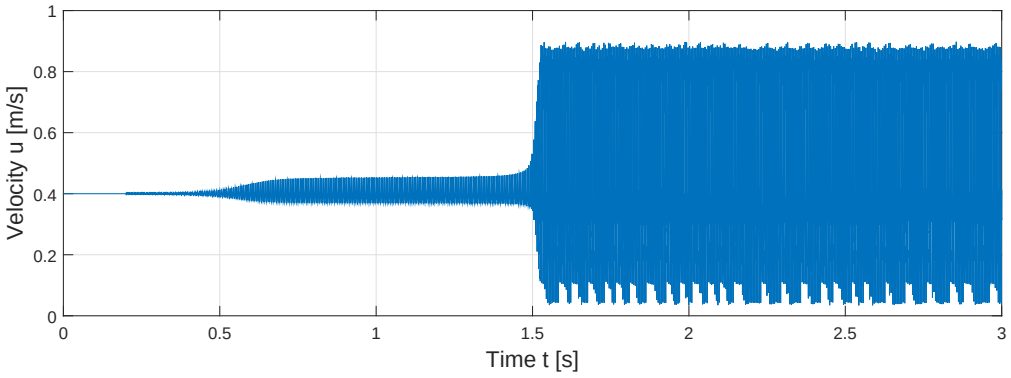

Figure 2.6: Example of a signal with two different amplitudes. First an oscillation with a small amplitude evolves and stabilizes. Then another frequency gets dominant and the amplitude changes again.

One of the best known thermoacoustic system which becomes theromacoustically unstable is the so-called 'Rijke tube'. It was considered in many studies (see e.g.Heckl (1988)) and is a simple example to explain the thermoacoustic feedback loop of a system as in Polifke (2004). It is basically a tube with open ends at both sides and a heat source at a fourth of the tube length. A very similar system was considered by Kashinath et al. (2013a).

2.5.2 Rayleigh Criterion

To predict the stability or instability of a thermoacoustic system it is necessary to look at the heat release and the pressure behaviour relative to each other. Rayleigh (1878) was the first who postulated a criterion which can be used to predict thermoacoustic instabilities. It can be written as an integral shown in equation (2.33) (see e.g. Polifke (2004)).

$$\oint p' \cdot \dot{Q}' d\,t > 0 \tag{2.33}$$

Basically the criterion means that the pressure fluctuation p' and the heat release fluctuation $\dot{Q}'$ have to be in the same phase to get an unstable system behaviour. As interpreted by Polifke (2004) this means that the heat release must be large at the highest compression during one cycle. So the amplitudes grow over each cycle. In a non-linear system this means it grows until the non-linear element saturates and a stable oscillation can evolve.

2.5.3 Analysis methods

There are several possibilities to analyse the gained results from a thermoacoustically oscillating system. One important signal is the velocity graph. It shows the reference velocity changing over time. An option is to do a Fast-Fourier-Transformation (FFT) of the signal to get the frequencies with which the system oscillates. So it is also possible to calculate the period time τ of the dominant frequency just by using equation (2.34).

$$\tau = \frac{1}{f} \tag{2.34}$$

This parameter is also important for another analysis method called a 'Phase Portrait'. Here the values of $u(t)$, $u(t-\tau)$ and $u(t-2\tau)$ are plotted in a 3D-Plot. Some examples of such phase portraits are in chapter 5 and chapter 6. The phase portraits can be used to identify the oscillation type. The different types are described in 2.5.4.

2.5.4 Different Oscillation Types

There are basically four different types of oscillations in unstable thermoacoustic systems as described by Orchini et al. (2015). They are:

- Chaotic Oscillations
- Frequency-Locked Oscillations
- Quasiperiodic Oscillations
- Limit Cycle Oscillations

In Orchini et al. (2015) all types can be found with an example plot. As described before, the phase portrait plot is used to identify the oscillation type. Chaotic oscillations do not have a regular path in these plots. They change their path randomly. The intersection of the paths with the zero level of the $u(t-2\tau)$ direction is also an indicator for the oscillation type. In this 2D plot the intersections are also randomly distributed.

The second oscillation type is a frequency-locked oscillation. This type has a dominant frequency but also other overlaying frequencies which disturb the path in the phase portrait, so the path starts to scatter. After a certain amount of periods the path repeats itself exactly again.

A quasiperiodic oscillation is the third type. It is pretty much the same as the frequency-locked type. The only difference is that the path never repeats. So the paths scatter around a dominant path just as the frequency-locked type.

The last type is a limit cycle oscillation. This oscillation has a dominant frequency and in most cases their higher harmonics are also present. In the phase portrait plot the path repeats itself every cycle. This can also be seen in the 2D intersection plot. There the intersections do not scatter. They are all overlain located at certain intersection points.

3 Software

The computation of the thermoacoustic systems described in this thesis was done by two different programs. The first is a Level-Set solver called 'GFlame' developed by Steinbacher (2016). It can compute the movement of the flame surface of a laminar premixed flame. The numerical solver included in this program was made by Mitchell (2008). The other program to cover the acoustics is called 'taX'. It was developed by Emmert et al. (2014) and it uses a low-order network model. These two programs were coupled to gain thermoacoustic oscillations. In this chapter, the programs are briefly described and the coupling is explained.

3.1 GFlame

GFlame is a Level-Set solver which computes the behaviour of a flame. The flame is modelled as a discontinuity between the unburned and the burned gas. This border is described by the G-field. GFlame is a 2D solver which means that the G-field is a surface which moves in a 3D space. It is described by equation (2.2). At the intersection of the G-field with the zero layer in the third dimension, the flame surface is formed. Since the G-Equation is a non-linear partial differential equation (PDE) which cannot be solved with analytical methods, a numerical method is needed to get approximated values. The commonly used method for the G-Equation is the Finite-Difference method. In this method the derivatives are approximated by differences. Space and time discretization can be treated differently. The numerical schemes used by GFlame are the TVD integration method for the time step and the WENO scheme for space discretization. Both methods are described in the following chapters.

3.1.1 Principle of Operation

First the general process of GFlame is considered. It is shown in figure 3.1. At the beginning the case is set up. This means the configuration files are loaded. These files contain information about the solving method, the boundaries, the velocity model and the flame properties. The different configuration options are outlined later. The information are merged to a structure called 'GFcase' which is committed to the numerical solver. Next the output file gets prepared and CFD data is loaded if it is needed. Now the solver parameters are set based on the informations from the GFcase.

The next part is the time integration loop which runs from the given start time to the given end time. In this loop every cycle a predefined time step is computed. These predefined time steps consist of several full time steps generated by the solver itself. All full time steps are split into three sub steps. The second and third sub step are updated based on the prior sub step.

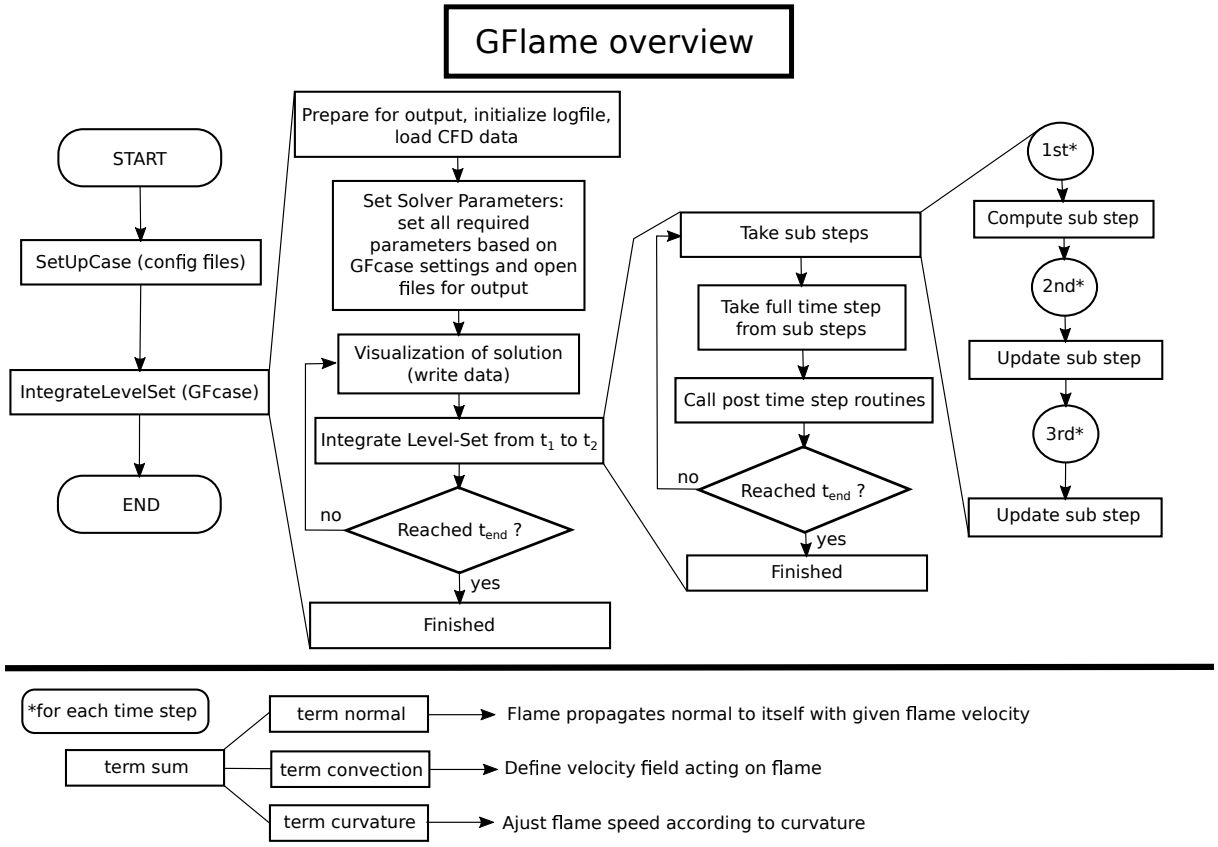

Figure 3.1: Flow chart of the Level-Set solver.

For each sub step the space discretization is performed. The discretized term is called term 'sum'. It consists of three smaller terms. The term 'normal' describes the flame propagation normal to the flame front, term 'convection' covers the velocity field and term 'curvature' changes the flame speed depending on the curvature. With the three different time sub steps a full time step is taken and the needed solvers are loaded and applied. Then the program checks if the predefined time step is reached. For each predefined time step the data is written into the output files and is also visualized. Both of these functions can also be switched off. After reaching the defined end time the program has finished.

3.1.2 Numerical Schemes

As spatial discretization for the solver used in this thesis, 'Weighted-Power-Essentially-Non-Oscillatory (WENO) Schemes' fifth-order accuracy are used. Basically a third-order ENO scheme is applied with limitiers attached to the used second-order differences. Additionally a weighting strategy is adapted to enhance the accuracy to fifth-order. The scheme is detailed described by Serna and Qian (2006).

After discretizing the spatial derivatives, the equation turns into a system of ordinary differential equations (ODE). Such a system can be written as in equation (3.1).

$$\frac{\partial u}{\partial t} = L(u) \tag{3.1}$$

To solve such a system, a 'Total-Variation-Diminishing' (TVD) Runge-Kutta scheme was used (see e.g. Gottlieb and Shu (1998)). The main difference between this scheme and other schemes is that the total variation does not increase for the next time step. The total variation is calculated with equation (3.2).

$$TV(u) = \sum_i |u_{i+1} - u_i| \tag{3.2}$$

Now for each time step equation (3.3) must be valid.

$$TV(u^{n+1}) \leq TV(u^n) \tag{3.3}$$

The TVD scheme was used to damp the results and to avoid non-physical oscillations of the solution. It is a method which is very stable, also if the solution shows an oscillation behaviour.

3.1.3 General Settings

The solver GFlame can be configured by three different input files. The first is the file 'settingsExample'. Therein some basic configurations can be made. First of all the flame type can be chosen here. It is possible to use a conical or a slit flame. In chapter 5 a conical, in chapter 6 a slit flame is used. Next configuration option is whether the simulation is done for the full flame or if the symmetry is utilised. The symmetry option spares computational time and should be used if possible.

In this file also the properties of the unburned gas are set. The required values are the temperature, the pressure and the kinematic viscosity. Also the laminar flame velocity is defined here. It is possible to insert this value manually or by defining the unburned gas mixture and the mean equivalence ratio and the program calculates s_L by using a correlation as in equation (2.3) for a methane air mixture.

The next parameter which can be specified here is the mean axial flow velocity at the inlet. In order to cover curvature effects the Markstein length (see e.g. Orchini et al. (2015)) can be defined here. It is also necessary to activate the curvature effects which is described later. A parameter which covers the expansion of the gas after it is burned is the volumetric expansion ratio $E = \frac{\rho_h}{\rho_c}$. It defines the change of the density after the combustion.

The last values which are defined in this file are geometric parameters. Here the radius of the feed channel is defined. This radius is in most cases equal to the radius of the flame r_f. With the lateral offset parameter the flame radius can be changed without modifying the feed channel radius. The lift off of the flame can also be defined here. It describes the distance of the feed channel to the flame in flow direction.

3.1.4 Solver Settings

The second input file which is needed is the file 'settingsSolverExample'. In this file the solver can be configured. First the curvature can be activated. If the calculation is done with curvature the Markstein length has to be set as described in chapter 3.1.3. The computation with curvature needs far more time than without it. That is the reason why it was not used in this thesis. Also it was not used in the reference cases from chapter 4 published by Kashinath et al. (2013a). Another configuration option is the initial condition of the simulation. It is possible to choose between a 'default' setting which means that the program first creates a new case and a 'resume' setting which continues the computation of an already existing case. The resume option was used for the examples in chapter 5 and chapter 6 to get a stable initial position for the coupled simulations.

As for every transient simulation, a start time and an end time must be defined. This is also done in the solver settings file. In fact the time step is changing like described in chapter 3.1.1. This means that the end time is eventually not reached exactly. The maximum deviation for this value is also defined here.

Another important value called the CFL-number can also be specified in this file. Equation (3.4) shows the definition of the CFL-number

$$0 \leq CFL = \frac{u \cdot \Delta t}{\Delta x} \leq 1 \tag{3.4}$$

The CFL-number describes the relation between the time step, the space step and the flow velocity. It is an important value to predict the stability of the numerical solving scheme for hyperbolic partial differential equations. The value must be between 0 and 1 and $CFL = 0.5$ is a good first guess. A more detailed description is given by Ferziger and Perić (2008) and by Hirsch (2007).

Next the accuracy can be specified. There are four different options for the accuracy which are 'low', 'medium', 'high' and 'veryHigh'. Each of this levels has another discretization scheme. The accuracy 'veryHigh' was used to generate the data described in this thesis. This is the scheme which is described in 3.1.2. The lower schemes need less computation time. They were used for the first simulations to do a coarse analysis of the systems. Then the data was recalculated with the most accurate scheme.

The spatial discretization configuration can also be done here. In order to discretize the field the spatial step is defined. It is the same for the x-direction and the y-direction. In this file the output is also specified. The number of output steps or the limits of the plots were also defined here. In this file it is possible to do other configurations as reinitialization of the G-Field but it is too much to describe it here in detail.

3.1.5 Velocity Model Settings

The last file which has to be configured to set up a GFlame simulation is the file 'settingsVelocityModelExample'. Here the velocity model can be defined and configured. The first configuration is the type of the velocity model. The single types are described in chapter 2.2. Further-

more it is possible to choose between a transient and a constant simulation. In the transient case different types of input sources can be chosen. The options are listed in table 3.1.

Table 3.1: Options of the input source for a transient velocity model.

Type	Description
file	Load CFD data
harmonic	Generate a harmonic sine oscillation
sweep	Generate a Sine-Sweep velocity field to identify the non-linear system
broad	Generate a quasi-random velocity field to identify the linear system
step	Generate a jump of the velocity to analyse the step response
TaX	Couple in a State-Space system

Now in this file the special input parameters needed for the chosen configuration from table 3.1 can be set. These values are for instance the frequency of the velocity perturbation or its amplitude. Also the paths for the external files are specified here. For the sine sweep the minimum and the maximum frequency but also the number of periods can be defined. An important value for the coupling with taX is the mean surface of the flame which is also set in this file.

3.2 taX

In order to model the acoustics a program called 'taX' was used. It was developed and described by Emmert et al. (2014). The program is based on a low-order network approach. The fundamentals therefore are described in chapter 2.3. It uses 1D linearised wave equations. The setup is done in Matlab Simulink. This program is used to model and analyse linear acoustic and linear thermoacoustic systems. A further application is the export of State-Space models which can be imported in GFlame.

3.2.1 Simulink Setup

First the acoustic system is configured in Matlab Simulink. For that the program has to be in the activated path of Matlab. The elements which can be used are located in the 'taxLibrary' file. The elements used in this thesis are described in chapter 2.3. They are connected via the Riemann invariants. An example for such a setup is given in figure 3.2.

Here a flame with a reference element is positioned between two tube elements and at both ends boundary elements were placed. For the flame reference there are different elements that can be used. Two of them were used in this thesis. The first is a $n-\tau$ model as described in 2.3.4. It can also be deactivated to export a State-Space model as described later. The second reference element which was used is the generic reference model which can couple in a FTF file. After configuring the system in Matlab Simulink it is necessary to set up a

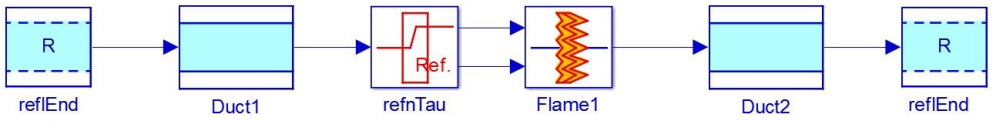

Figure 3.2: Example for a taX setup in Matlab Simulink.

Matlab file which calculates and manipulates the system. In this file first the maximum frequency is defined to which the system is analysed. Then the system is called by the function 'tax'. Now the acoustics can be analysed.

3.2.2 System analysis

In order to analyse a system, Matlab and taX provide a set of functions to visualize the acoustics. Most important are the eigenvalue plots to analyse the stability of the system. It is critical that the real parts of all eigenvalues are negative or close to the imaginary axis if they are positive. The eigenvalue plots are the first reference point for designing a potentially oscillating system.

Next the eigenfrequencies can be analysed. Therefore it is possible to plot the amplitudes and the phases of the velocity fluctuations and the pressure fluctuations at the eigenfrequencies. The amplitudes of the velocity fluctuation of the system described in figure 3.2 are plotted in figure 3.3.

This figure is used to analyse the eigenfrequencies, which are a first guess at which frequencies the system will start to oscillate. It is also important to consider the amplitudes itself. The highest amplitude is an indicator for the eigenfrequency that evolves as the dominant frequency in the coupled system.

After the setup is done and the acoustics simulation has finished, taX has generated a 'Multiple-Input-Multiple-Output' (MIMO) system. Now it is possible to extract a State-Space system which is a SISO system. In this thesis a system which gets the normed heat release fluctuation of the flame element as an input is needed. As described in chapter 2.4.1, the input is equal to the normed flame surface fluctuation which is calculated by the Level-Set solver. The output of the SISO system is the normed velocity fluctuation. This value is later used to construct the velocity field in GFlame.

3.3 Coupling of GFlame and taX

A thermoacoustic oscillation can be simulated by combining the non-linear Level-Set solver GFlame with the acoustics software taX. Therefore a State-Space system is generated with taX as described in chapter 3.2.2. This system is used to generate a velocity field in GFlame. For the simulation a convective velocity field type is used as mentioned in chapter 2.2.2 but now

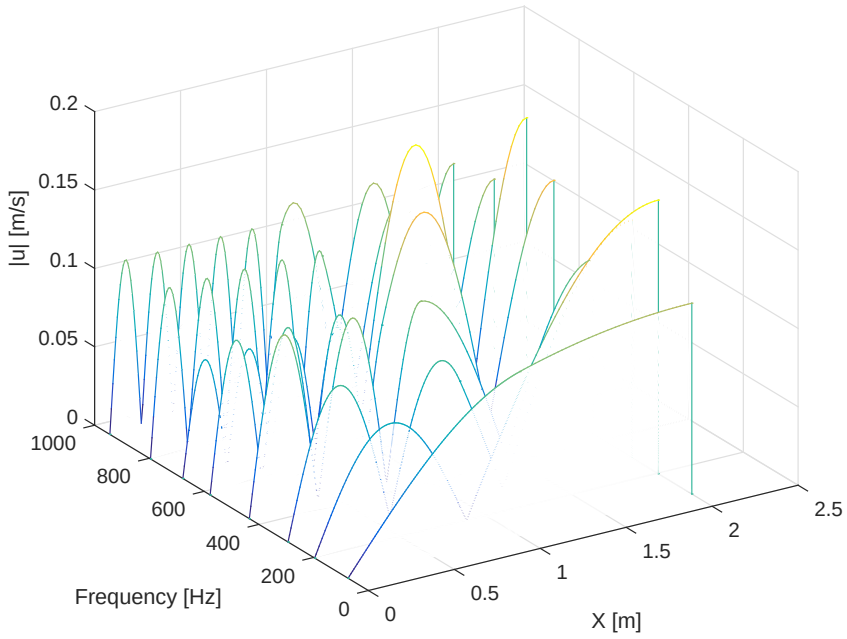

Figure 3.3: Example of a velocity fluctuations plot where the eigenfrequencies can be seen.

the fluctuation is not sinusoidal. The velocity fluctuation is calculated by the acoustic State-Space system and is depending on the current heat release of the flame. The acoustic system needs the normed heat release fluctuation $\dot{Q}^*$ which is equal to the normed surface fluctuation A^*. With the normed surface fluctuation of the flame the normed velocity fluctuation is calculated. This leads to a feedback loop as shown in figure 3.4. It is a very basic thermoacoustic feedback loop. A more detailed loop which also implies other effects and a description of the control theory behind such a system is explained by Polifke (2004). A general description of feedback loops can be found in Lunze (1996)

This feedback loop was implemented in Matlab as a function of GFlame. This function must provide a velocity vector for a given time vector. This time vector is basically the time lag between a certain point of the velocity field in flow direction and the reference point subtracted from the current time. The time lag can be computed with the distance between the searched point and the reference point and the convective velocity which is in most cases the mean flow velocity. The flow chart in figure 3.5 shows the principle of this function.

First the function gets the current time and compares it with the time vector. So the first cycle can be evaluated. If it is the first cycle the function returns just the mean velocity. If the simulation is resumed and there are enough data points the velocity vector is interpolated. If it is not the first cycle a time vector is resampled from the first time point to the current time. Then the polynomial order is set to a desired value. This value defines the type of polynomial function which is used to fit the surface data. Then the data length is defined for a least square fit. In the used configuration in chapter 5 and chapter 6 the polynomial function was second

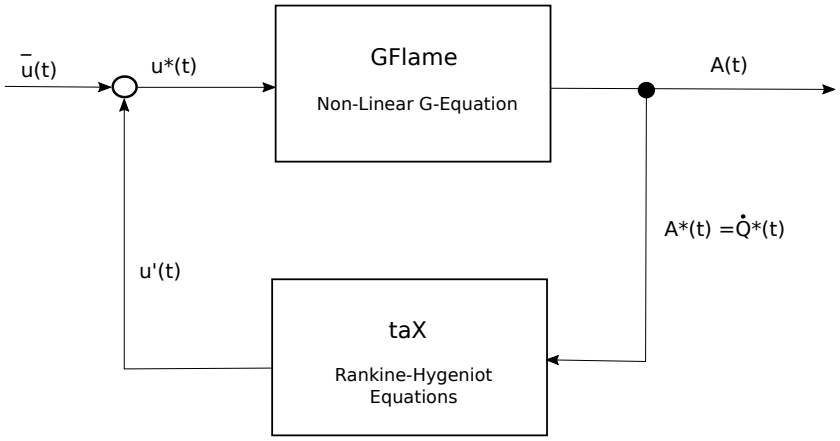

Figure 3.4: The feedback loop of the thermoacoustic system.

order which means it is quadratic. The number of required points for the least square fit was specified as 9. This was done because a quadratic function needs 3 points to be defined and the number was tripled to smooth the resulting function. Now the program checks whether enough data points from previous cycles are available. If not the order is reset to 0 and 2 data points were chosen.

After the configuration of the polynomial order, the matrix for a least square fit is built up and solved. Now the coefficients of the polynomial function are known. Next the polynomial function is used to calculate the new flame surface area for all time points which were resampled in this cycle. Then the surface points are normed as described in equation (2.32). These normed surface fluctuations are now used as input signal for the State-Space system generated by taX. The result is a normed velocity fluctuation vector. The State-Space system needs a initial condition as written in equation (2.24). So for the next cycle the result of the current State-Space vector is computed during the simulation of the velocity fluctuation. This vector now is stored as new initial condition for the next cycle. Next step is to attach the new gained data points to the already existing values. The last step is to interpolate the velocity vector with the new velocity and time vector.

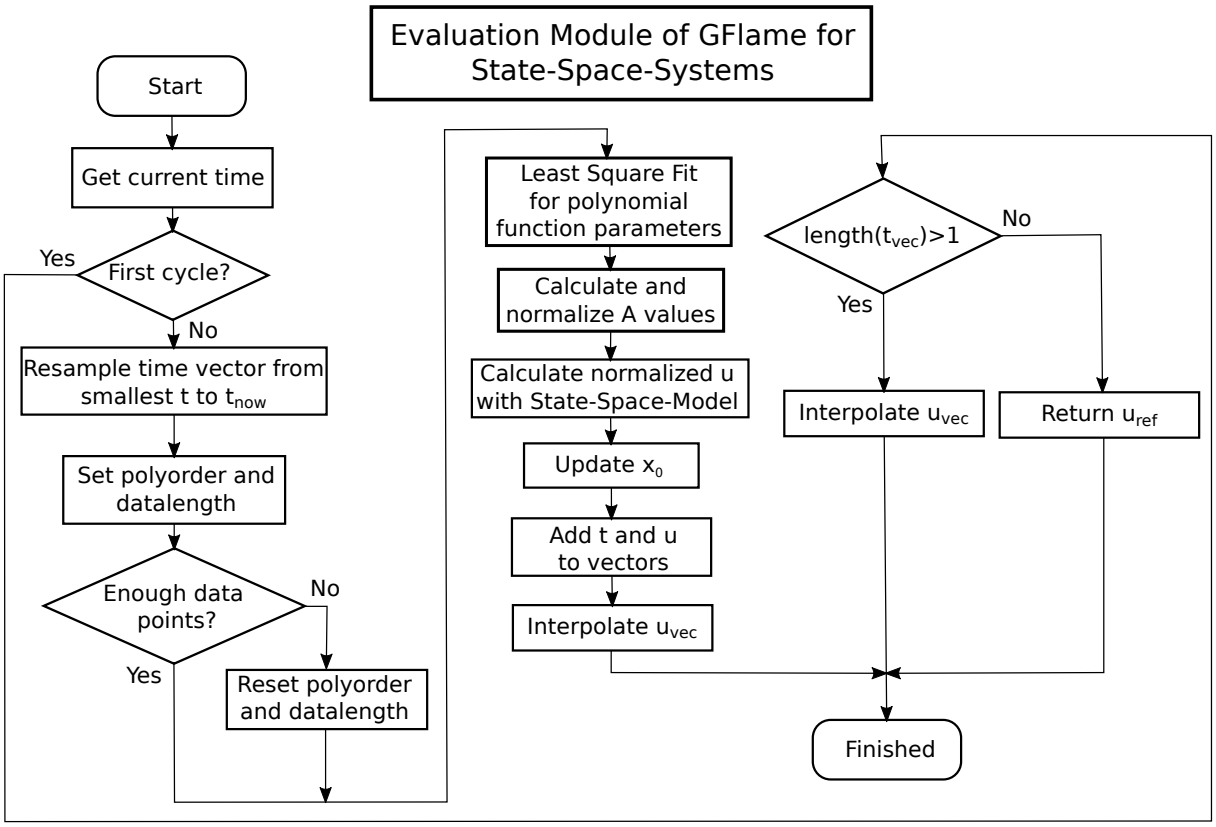

Figure 3.5: Flow chart of the coupling module.

4 Verification of GFlame

In this chapter the verification of the Level-Set solver GFlame is described. In order to achieve this goal, results from Kashinath et al. (2013a) were used. The input parameters were reconstructed to be able to configure GFlame. Then the gained results were compared to the results published by Kashinath et al. (2013a). For comparison two different cases were chosen. The first is a verification of the flame contours and the second is a comparison of the Flame-Describing-Function.

4.1 Flame Contours

The first verification was done by reconstructing the flame contours published by Kashinath et al. (2013a). In this publication the author used a very similar solver to GFlame. Furthermore the velocity field is a convective type as GFlame can handle. First task was to construct the input parameters because in the publication only non-dimensional values were used. Then the simulation was done and the flame contours were compared.

4.1.1 Construction of the Input Parameters

First the input parameters are evaluated. The given parameters from Kashinath et al. (2013a) are listed in the table below:

Table 4.1: Given values for test setup with convective velocity field.

Name	Value
Equivalence ratio	$\Phi = 1.06$
Laminar flame velocity	$s_L = 0.42\,\mathrm{m/s}$
Flame aspect ratio	$\beta_f = 2.14$
Amplitude of the velocity perturbation	$\epsilon = 0.25$
Phase speed of velocity perturbations	$K = 2.5$
Strouhal number	$St = 1$

With these parameters the task was to reproduce the same results in order to check the proper implementation of GFlame. In the publication the flame contours are given at six specific angles of the forcing cycle. Also the pictures were taken after the initial conditions had no measurable influence on the shape. The results shown in figure 4.4 were published in Kashinath et al. (2013a).

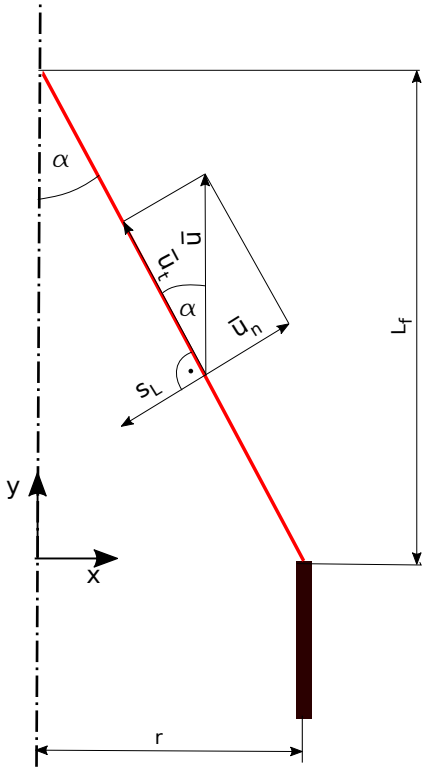

Figure 4.1: Scheme of the geometric and the velocity triangles.

Since GFlame works with dimensions and the present results from the paper are non-dimensional, the assumption was made that the radius of the burner is fixed at $r_f = 1\,\text{mm}$. All other values can be calculated based on this restriction.

First $\bar{u}$ was calculated by the following consideration. In steady state the flame, without any curvature influence, shapes a cone. With the known flame length and the given radius it is possible to calculate the flame cone angle α. The relation is given in equation (4.1).

$$\tan(\alpha) = \frac{r}{L_f} \tag{4.1}$$

Afterwards the ratio of $\frac{r_f}{L_f}$ can be replaced by $\frac{1}{\beta_f}$. The next step is to build up a kinematic triangle at the surface of the flame. As first step the mean flow velocity $\bar{u}$ is fixed on the surface of the flame and points in y-direction. Then it is dismantled in a normal component $\bar{u}_n$ and a tangential component $\bar{u}_t$. Because of the congruence of the kinematic and the geometric triangle the angle α is the same. Next the magnitude of the normal component and the flame velocity are the same. Figure 4.1 shows the geometric and the kinematic relations.

For the kinematic velocity triangle the trigonometric equation is given in (4.2).

$$\sin(\alpha) = \frac{\bar{u}_n}{\bar{u}} \tag{4.2}$$

With all these assumptions it is easy to merge them to equation (4.3) for $\bar{u}$. It depends only on the flame velocity and the flame aspect ratio β_f.

$$\bar{u} = \frac{s_L}{\sin\left(\arctan\left(\frac{1}{\beta_f}\right)\right)} \tag{4.3}$$

Now the flow speed can be calculated and the result is $\bar{u} = 1\,\mathrm{m/s}$. The next parameter which was needed is the forcing frequency f_{exc}. It can be determined by the use of the Strouhal number $St = \frac{f \cdot L_f}{\bar{u}}$. So the forcing frequency has a value of $f_{exc} = 467\,\mathrm{Hz}$. At this point each needed input value is specified. They are summarised in table 4.2.

Table 4.2: Input parameters for GFlame simulation.

Name	Value
Laminar flame velocity	$s_L = 0.42\,\mathrm{m/s}$
Flame radius	$r_f = 1\,\mathrm{mm}$
Mean flow velocity	$\bar{u} = 1\,\mathrm{m/s}$
Velocity perturbation	$\epsilon = 0.25$
Phase speed of velocity disturbances	$K = 2.5$
Forcing frequency	$f_{exc} = 467\,\mathrm{Hz}$

4.1.2 Results with a Convective Velocity Field

A simulations with the constructed input parameters was set up. The results of Kashinath et al. (2013a) are shown in 4.4. It is important to mention that it is not the first cycle of the simulation. The plotted cycle is one after the system has settled in a periodic transient state.

Now the same case was computed by using GFlame as a solver. The results for the reference velocity and the flame surface plotted over time are in figure 4.3.

As already mentioned the flame needs a few cycles to get into a stable cycle. Next step is to investigate one of the forced cycles using GFlame. Because of a mathematical different velocity field between the solver used in Kashinath et al. (2013a) and GFlame, the cycle does not start at 0°. The first curve was fitted and then the other curves were computed over one cycle. This means that the definition for 0° differs between the results gained by Kashinath et al. (2013a) and the results computed with GFlame. The results are shown in figure 4.2.

The curves were plotted in the same style as in Kashinath et al. (2013a) to simplify the comparison. Therefore the flame was also elevated. The chosen offset is 0.45 mm. The pictures shows that the results of both solvers are almost identical.

4.2 Flame-Describing-Function of a Conical Flame

As a second verification approach the Flame-Describing-Function (FDF) was considered. In Kashinath et al. (2013a) the FDF was computed with pretty much the same input as for the

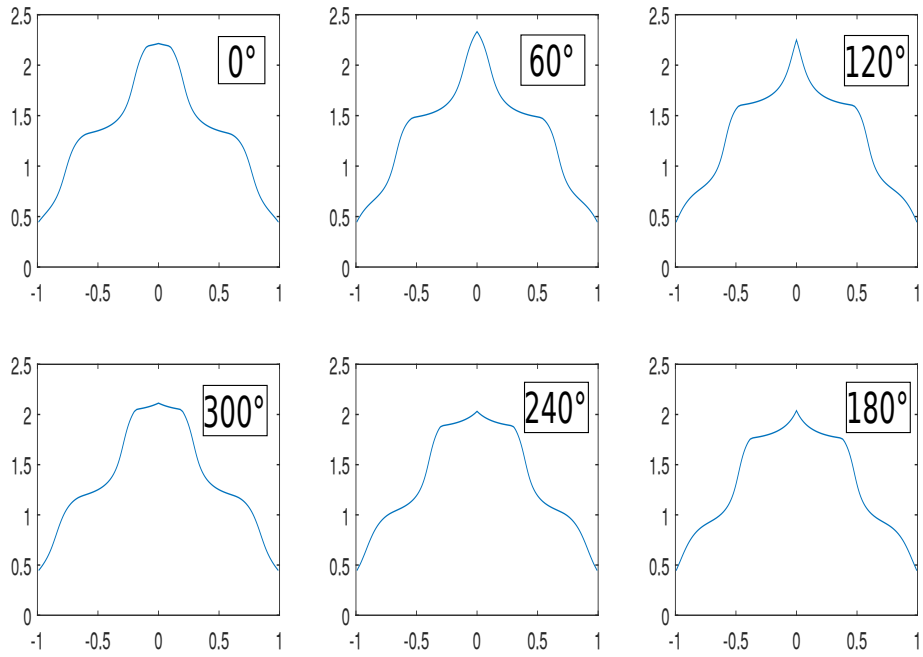

Figure 4.2: Resulting curvatures from the GFlame simulation.

flame curves in the previous section. The simulation was done with different Strouhal numbers from $St = 0$ to $St = 4$. This was done for specific perturbation amplitudes. The results from Kashinath et al. (2013a) are depicted in figure 4.5.

Here the gain describes the amplifying properties of the system between the input signal and the output signal. In this case the input signal is the normed velocity fluctuation and the output signal is the normed area fluctuation. The phase describes the shift of these signals. As described in chapter 2.4 the transfer function depends on the forcing frequency but also on the amplitude of the inlet signal which makes the system non-linear. In order to get comparable results, the input parameter from 4.2 are chosen with a few exceptions. First the frequency of course changed over the simulation. Also the amplitude ϵ was varied. Due to limited computation time the simulation was split into different simulations in which the input parameters were adapted to reduce the overall computational time. Also only the frequency range from 0 Hz to 1000 Hz or form $St = 0$ to $St = 2.14$ was observed.

For each amplitude a separate simulation was done. The amplitudes were chosen as shown in Kashinath et al. (2013a). These simulations were also splitted into two separate ones with an adjusted number of periods for the velocity field. Lower frequencies need much more simulation time per period than higher frequencies but a lower number of periods sufficient. So first a simulation from the range of 0 Hz to 300 Hz was done with a period number of 3. Next the simulation was done from 300 Hz to 1000 Hz with a period number of 8 at the same amplitude. Then the resulting data points were merged to one curve.

In figure 4.6 the bode plot of the results is shown. At higher frequencies the data point scattering increases. To get more even results the number of periods has to be increased. In this case this trade off was done to achieve good results with acceptable time costs.

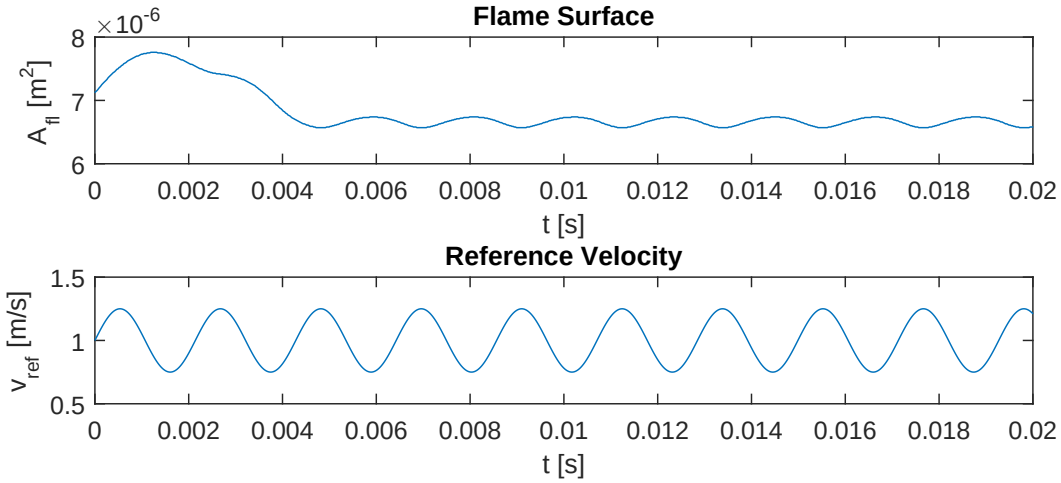

Figure 4.3: Reference velocity and flame surface area during a harmonic forced simulation.

The FDF results differ from the results gained by Kashinath et al. (2013a). For low ϵ the gain results match pretty well. The cut-off frequencies for $\epsilon = 0.02$ are at $St = 0.8$ and $St = 1.5$ which matches with the results from the literature. The gains for higher amplitudes are lower than in the gains published by Kashinath et al. (2013a) but the trend is comparable. The phase results differ more. Here the phase at low frequencies decreases much less than in the compared case. Also the phase jumps are not equal to the results from 4.5. The phase also decreases stronger for amplitudes of $\epsilon = 0.22$ and $\epsilon = 0.26$ than for $\epsilon = 0.4$. The opposite behaviour was expected. One possible reason therefore is that the spatial and time discretization has to be increased. Also the number of periods for the sine sweep should be increased. At higher frequencies the number of periods is too small as can be seen in the gain plot. Here the results start to scatter which is an effect of a numerical issue or a low number of periods.

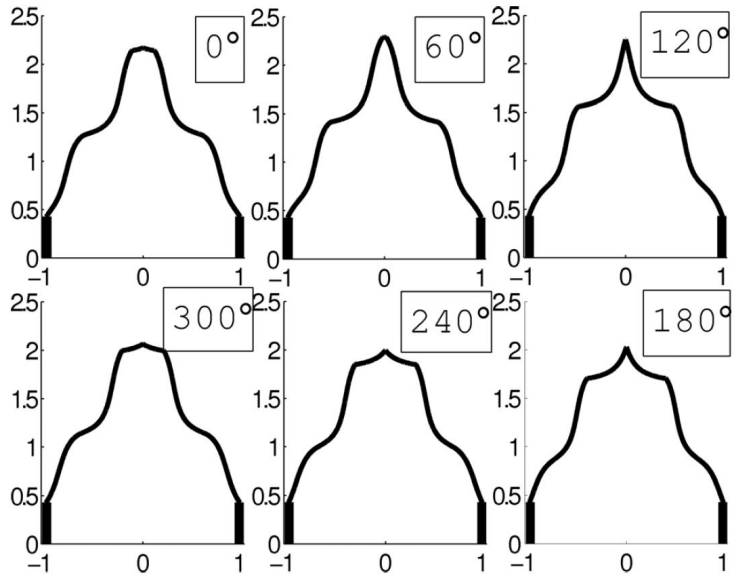

Figure 4.4: Flame curvatures at specific angles during one forcing cylce from Kashinath et al. (2013a).

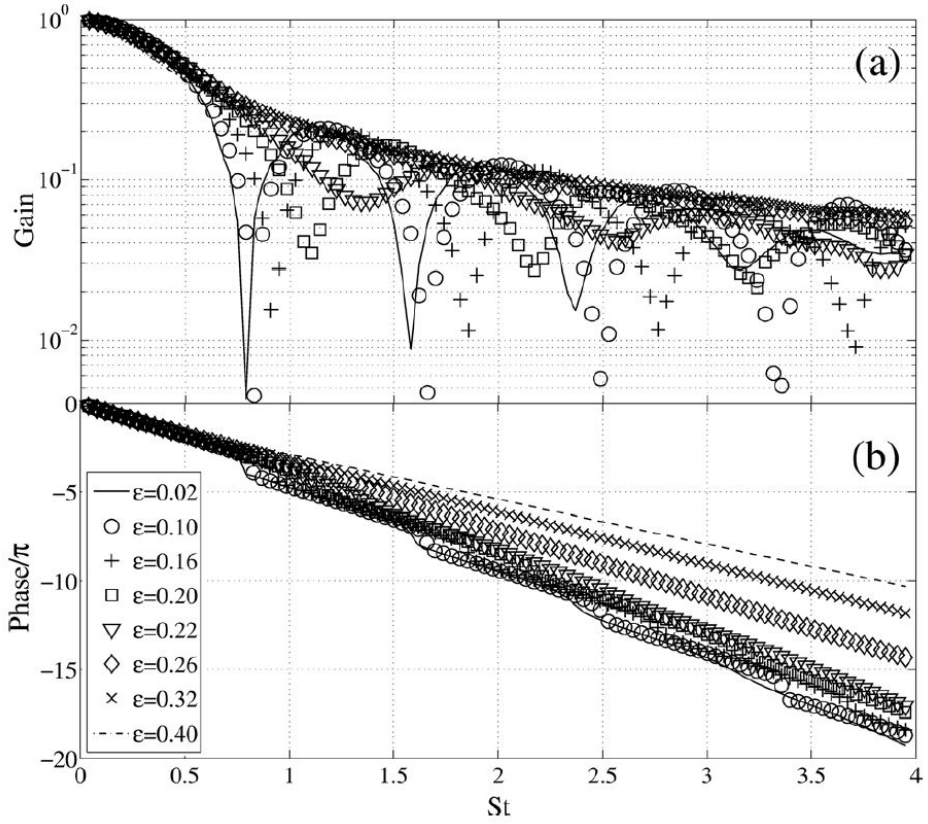

Figure 4.5: Flame-Describing-Function from Kashinath et al. (2013a).

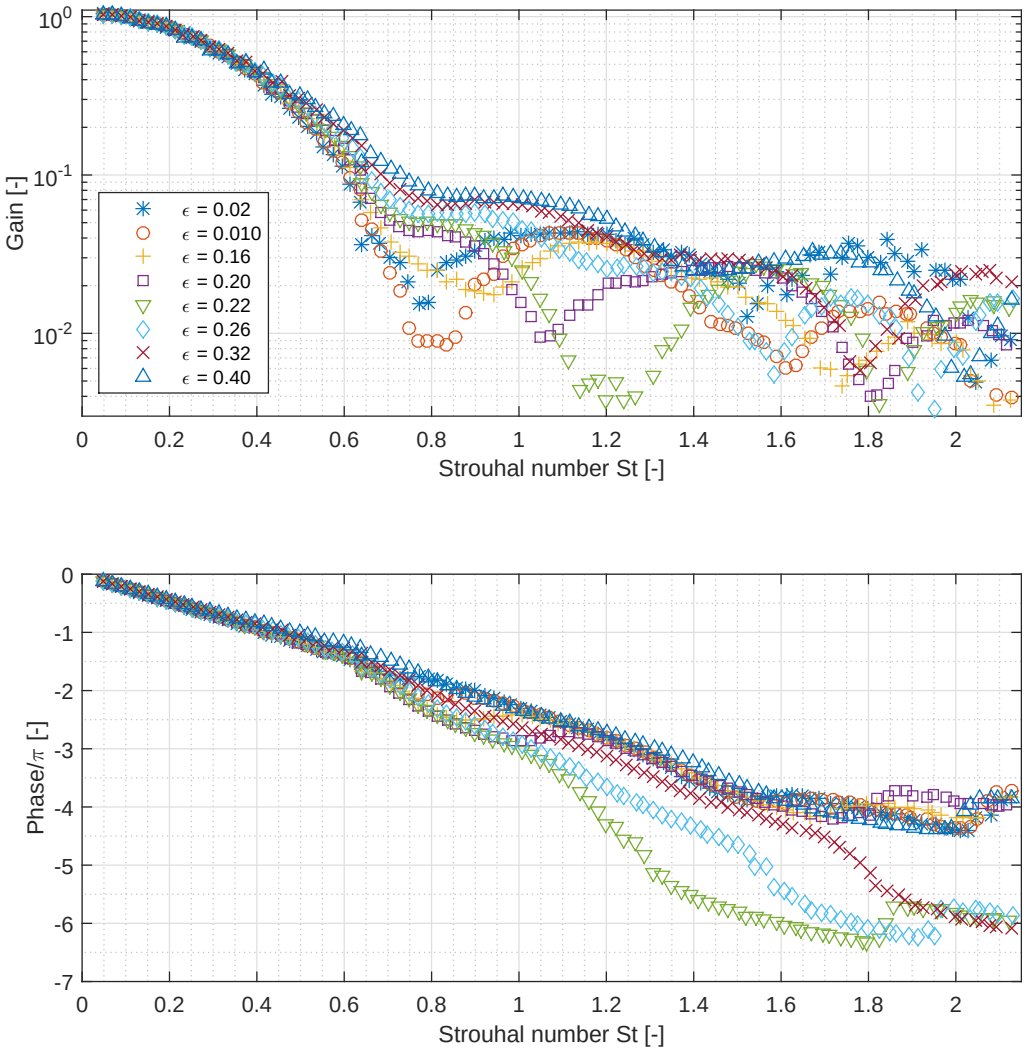

Figure 4.6: Flame-Describing-Function calculated with GFlame .

5 Coupled Simulation with a Conical Flame

In order to verify the implemented coupling between the Level-Set solver and the linear acoustics, a test case from Orchini et al. (2015) was used. This system was chosen due to its simplicity. Also the the used tools are similar to the tools used in this thesis. First the system was rebuilt with the software described in chapter 3. Then simulations were done for specific system configurations by changing the position of the flame. The results were analysed using FFT, bifurcation plots and phase portraits. Then the results were compared to the data gained by Orchini et al. (2015)

5.1 Setup Description

In Orchini et al. (2015) a system is described which is basically a tube with a conical flame in it. The interaction between the flame and the acoustics was analysed . Figure 5.1 shows the acoustic system which was used by Orchini et al. (2015).

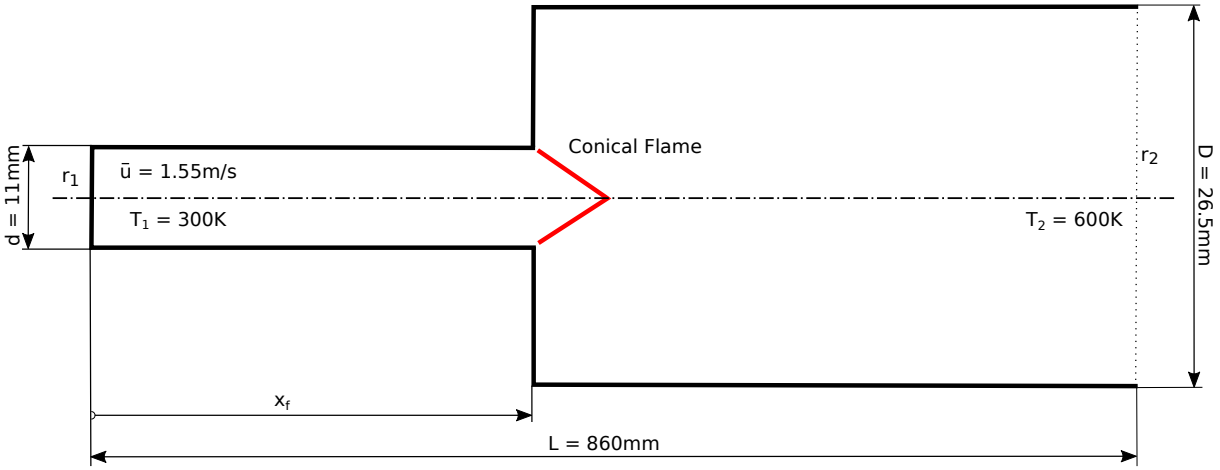

Figure 5.1: Thermoacoustic setup as used by Orchini et al. (2015)

It shows a tube with a closed end $r_1 = 1$ on the left side. Then there is an area jump at which the flame is positioned and a tube with a larger diameter is attached. The position of the area jump with the flame can be varied over the length of the system. On the right side there is a boundary r_2 which can be described with the equation (5.1).

$$r_2 = -(1 + 0.9 \cdot Ma) \cdot \left(1 - \frac{1}{2} \cdot \frac{\omega^2 \cdot R^2}{c^2}\right) \tag{5.1}$$

The system was modelled as in taX as a low-order network model. With this model a State-Space system was generated which was used by the Level-Set solver used by Orchini et al. (2015). For the velocity field a convective incompressible velocity model was implemented.

5.2 Acoustic Setup

In order to remodel the system the acoustics were modelled in taX. First the system was simulated without the flame to export a State-Space model with the normed heat release fluctuation as input and the normed velocity fluctuation as output. This model was loaded by GFlame to cover the acoustics in the flame simulation. Also the eigenvalues and the eigenmodes were analysed. Then an analytical linear flame model was exported from GFlame and loaded in taX. So the acoustic simulation was done again with an activated flame. This was done to compare the eigenvalues and eigenmodes of the acoustics with and without a flame. Later these values were also compared to the non-linear results of the coupled simulation.

5.2.1 System without Flame

To get a similar acoustic system, the case was modelled in taX. In figure 5.2 the used taX setup is shown. In this setup the flame is deactivated just to cover the acoustic behaviour. This is also necessary to be able to export a State-Space model from taX. Note that the boundary on the right side is fixed at $r_2 = -1$ which means that it is basically an open end boundary. That is just a simplification compared to the system from Orchini et al. (2015).

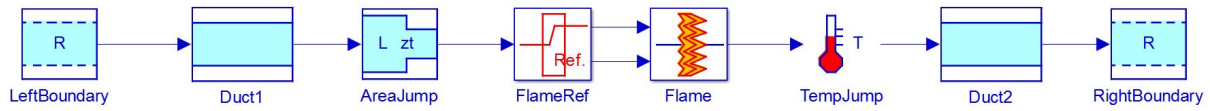

Figure 5.2: Acoustic setup in taX.

Table 5.1 contains all parameters used to set up the acoustic system. Here the Length L is the whole system length and the position of the flame is defined by the bifurcation value x_s. The small diameter at the inlet is d and the diameter at the outlet is D. The boundaries are specified by the values of r_1 at the inlet and r_2 at the outlet. Furthermore the input velocity $\bar{u}$ is fixed and its value is later used as the mean reference velocity in the Level-Set solver. In the tube the temperatures are given before the flame with T_1 and after the flame with T_2.

This taX system was used to generate the acoustic State-Space systems for different flame positions. The position was varied between 5% and 95% of the system length. Every 5% of L a step was taken. At 0% and 100% no steps were taken due to the fixed values of the acoustic variables which means that no oscillation is expected. The generated systems were checked

Table 5.1: Parameters of the acoustic network model.

Name	Value
Small diameter	$d = 11\,\text{mm}$
Larger diameter	$D = 26.5\,\text{mm}$
Length	$L = 860\,\text{mm}$
Left boundary condition	$r_1 = 1$
Right boundary condition	$r_2 = -1$
Mean inlet velocity	$\bar{u} = 1.55\,\text{m/s}$
Inlet temperature	$T_{in} = 300\,\text{K}$
Temperature jump	$T_2/T1 = 2$

for their eigenvalues and eigenmodes. For example the systems with the flame position at 10%, 40% and 70% of the system length L were chosen to show different behaviours. Figure 5.3 shows the eigenvalues of the three cases.

The real parts of the eigenvalues of all acoustic systems are negative. This means that the systems are stable. It is important to use stable acoustic systems because the system gets more unstable with an inserted flame. Such an eigenvalue shift is described in chapter 5.2.2.

Also the acoustic eigenfrequencies without flame were checked. They are plotted in the graphs in chapter 5.4 overlain to the simulation results. These frequencies are a first guess at which values the system starts to oscillate.

5.2.2 System with Linear Flame Model

For a more detailed analysis an analytic Flame-Transfer-Function was exported from GFlame as a State-Space model. This flame was configured like the flame setup for the non-linear simulation in chapter 5.3. In the taX system the flame was now inserted. Next the eigenvalues were analysed again to predict an oscillating behaviour. The change of the eigenvalues is plotted in figure 5.4.

Here can be seen that the eigenvalues shift in positive real direction. This destabilizes the systems. In the system with the flame positioned at 10% of the system length L, some eigenvalues are positive which means an unstable behaviour is predicted, but in chapter 5.4 the results show that the system is stable. The opposite is the case with the flame positioned at $0.4 \cdot L$. Here a stable system is predicted but the non-linear simulation starts to oscillate. In the last example the prediction of an unstable system is correct. With this knowledge it is possible to construct systems which are most likely able to oscillate. Important is that the acoustic system without a flame model has only eigenvalues in the negative real range. Some of them must be very close to the real zero line. With the non-linear flame model they shift to the real positive range and get unstable. Then they grow until the non-linearity saturates and a steady state oscillation has developed. If the acoustic system without a flame has already unstable eigenvalues it is most likely that they shift to higher real values and then the evolving oscillation is too strong to be covered with the Level-Set method. This means that the non-linear simulation does not work anymore.

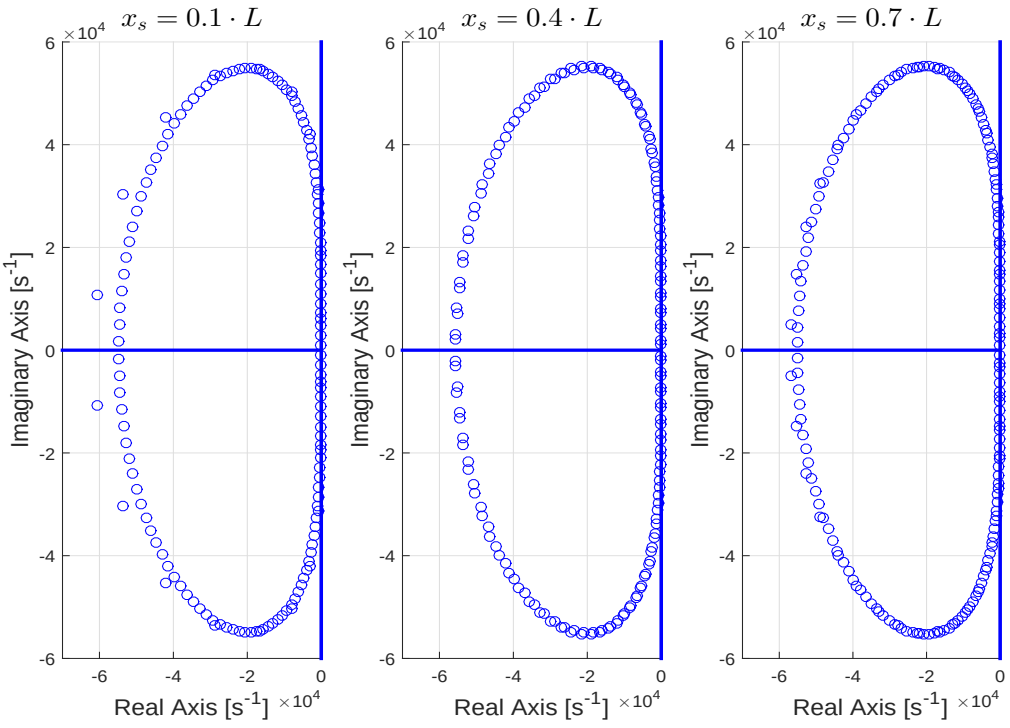

Figure 5.3: Eigenvalues of the acoustic system without flame.

5.3 Flame Setup

The used flame for the non-linear simulation was modelled with GFlame. In this case a cylindrical flame with a radius of 11 mm was simulated. This value was taken from the acoustics geometry. The main differences between the flame model used in this thesis and the flame model used by Orchini et al. (2015) are the velocity model and the curvature. The velocity model was changed from convective incompressible to convective and the curvature was disabled. This was done to reduce the computational time. Table 5.2 shows the main characteristics of the embedded flame. The unburned gas is a mixture of methane and air.

Table 5.2: Parameters of the flame model.

Name	Value
Flame radius	$r_f = 5.5\,\text{mm}$
Equivalence ratio	$\Phi = 0.51$
Flame speed	$s_L = 0.25\,\text{m/s}$
Mean flow velocity	$\bar{u} = 1.55\,\text{m/s}$

These parameters were used to compute a steady-state flame. A simulation duration of 0.2 s was chosen. The resulting flame is shown in figure 5.5. This steady state flame was needed to get the mean area value $\bar{A}$ for the coupled simulation. It is also necessary to start from such

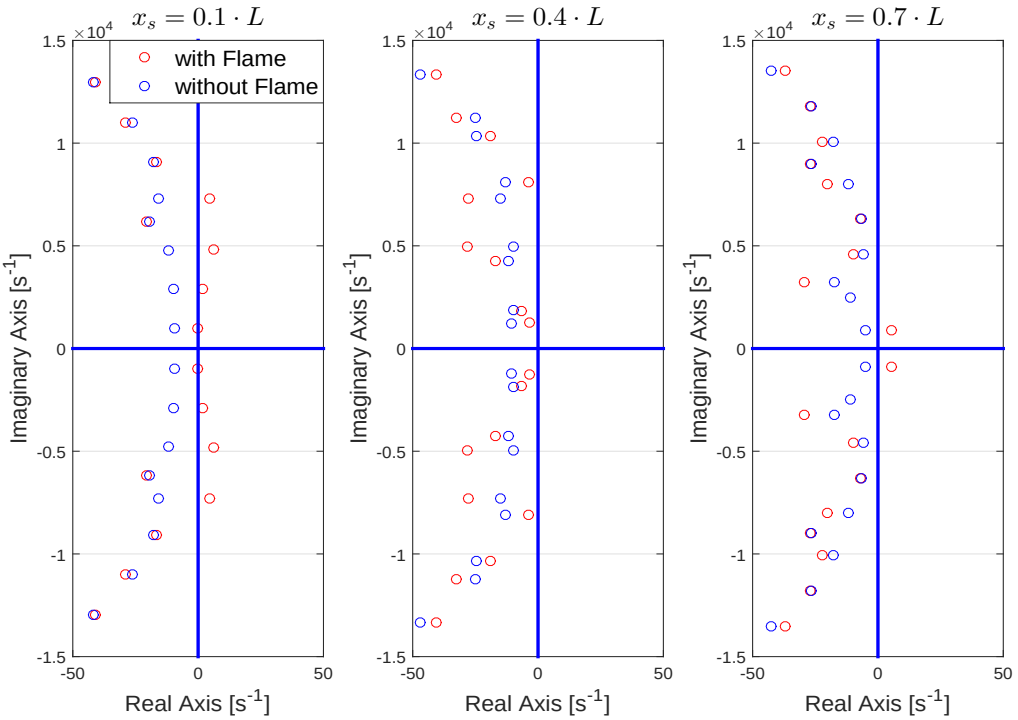

Figure 5.4: Eigenvalues of the acousitic system with and without flame element.

an unexcited state because otherwise all eigenfrequencies are strongly excited and the Level-Set solver overstresses and cannot compute meaningful results anymore.

In figure 5.5 only the upper half of the flame is shown because the simulation uses the symmetry of the flame to reduce the computational time. It is also possible to get the flame length L_f and to crosscheck the correct setup as described by the equation (4.3). The setup was also used to export the FTF for the linear analysis of the system. The bode plot of the FTF is shown in figure 5.6.

5.4 Simulation Results

The non-linear simulation was done with 19 different acoustic configurations as described in chapter 5.2. Then the results for each simulation were analysed using FFT and phase portrait plots. The three examples which are already used in chapter 5.2, are used to describe different system behaviour. Then the merged bifurcation data are shown and analysed.

5.4.1 Results for Specific Flame Positions

In order to compare the different systems the first approach is to look at the velocity signals and the flame surface signals. In figure 5.7 the signals are shown. For each case the first 0.2 s

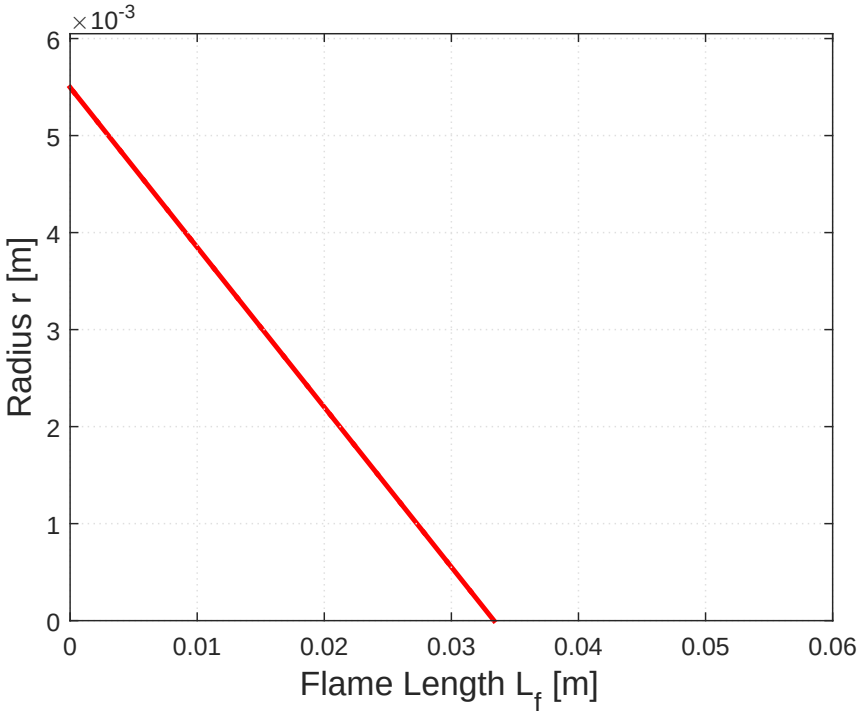

Figure 5.5: Default flame shape for the coupled simulations.

are the so-called 'default case' which is used to get a conical stable flame as a starting point. This is essentially because without this default starting point the flame can get so unstable that the flame contour moves outside of the grid of the solver and the results are not meaningful anymore. It is also necessary to get the mean flame surface which was taken to calculate the normed flame surface fluctuation as described by equation (2.32).

The signal at position $x_s = 0.1 \cdot L$ shows a stable system. The fluctuations of the area and the velocity signal are negligible. The signal noise is an effect of the discretization done by the Level-Set solver. A small error in the heat release leads to a small change of the velocity. Thus the signals starts to sweep. Due to the stable system this oscillation did not grow but it is the effect which leads to an oscillation in the other cases. Note that the flame surface signal is calculated at 0 s for a parabolic shape which is the initial condition as written in chapter 3. Then the flame gets into a conical shape which is the starting point of the coupled simulation. So the flame surface at the beginning is much larger than in the stable case. That is the reason why the area drops at the beginning.

With the flame positioned at $x_s = 0.4 \cdot L$ the system starts to oscillate. This can be seen in the velocity signal. First the velocity is constant at $\bar{u}$. Then it starts to oscillate triggered by the numerical noise. The amplitude increases up to a limit and then it oscillates onward. That is the expected behaviour of a limit cycle. Actually in this case it is not sure that it is a limit cycle. The reason for that is described later. The flame surface signal also shows the oscillations. Note that there is an area shift upwards depending on the current velocity amplitude but also

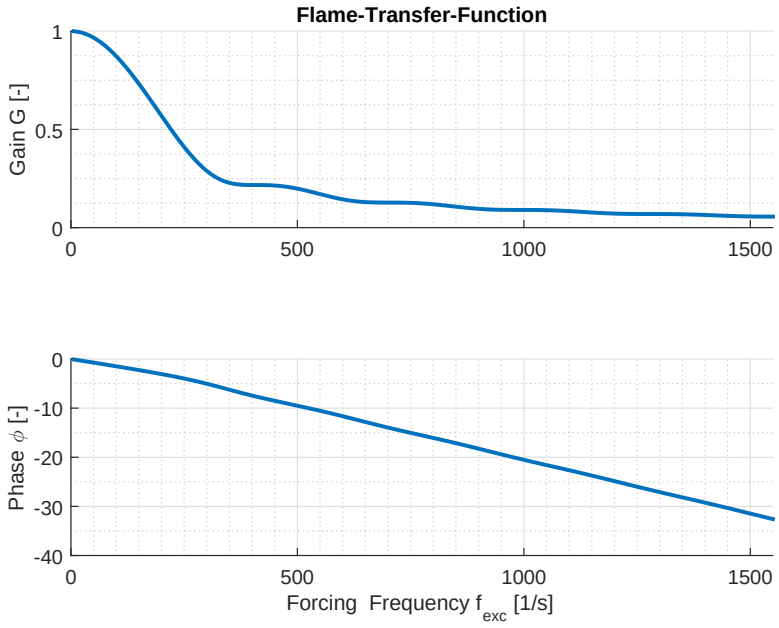

Figure 5.6: Gain and phase plot of the FTF used in the linear setup.

on the frequency of the velocity signal.

In the last described example the flame position is at $x_s = 0.7 \cdot L$. Here the behaviour is close to the system behaviour described in the passage before. The velocity amplitude reaches larger values but the system also needs more time to get in a steady-state oscillation. Compared to the case at $x_s = 0.4 \cdot L$ the velocity signal is much smoother. There are not so much higher overlain frequencies which disturb the signal. This leads to a limit cycle which is described later. With this configuration also the flame surface signal starts to oscillate and shifts to a larger mean value.

Now the signals were analysed by using FFT and phase portraits. First case is the example with the flame positioned at $x_s = 0.1 \cdot L$. In figure 5.8 the results are shown. In the detailed velocity signal plot it can be seen that there is just a weak noise signal. In the detailed area plot also the noise is shown. Here the discretization can be seen. This shows that the disturbance is very low. The FFT analysis of the signals show very low amplitudes. There is apparently no connection between the frequencies in the velocity and the area signal. This leads to the assumption that the oscillations are only caused by numerical issues. In both phase portraits the chaotic oscillations are also shown. In the velocity-area portrait also the numerical steps of the area signal can be seen. It also shows that the flame surface signal drops from a high value to the steady-state.

In figure 5.9 the results of the system with the flame flame position $x_s = 0.4 \cdot L$ are plotted. In the detailed plot it can be seen that the velocity signal is sinusoidal. In the detailed flame surface plot the signal is much more uneven. The trend of the signal is downwards. This means

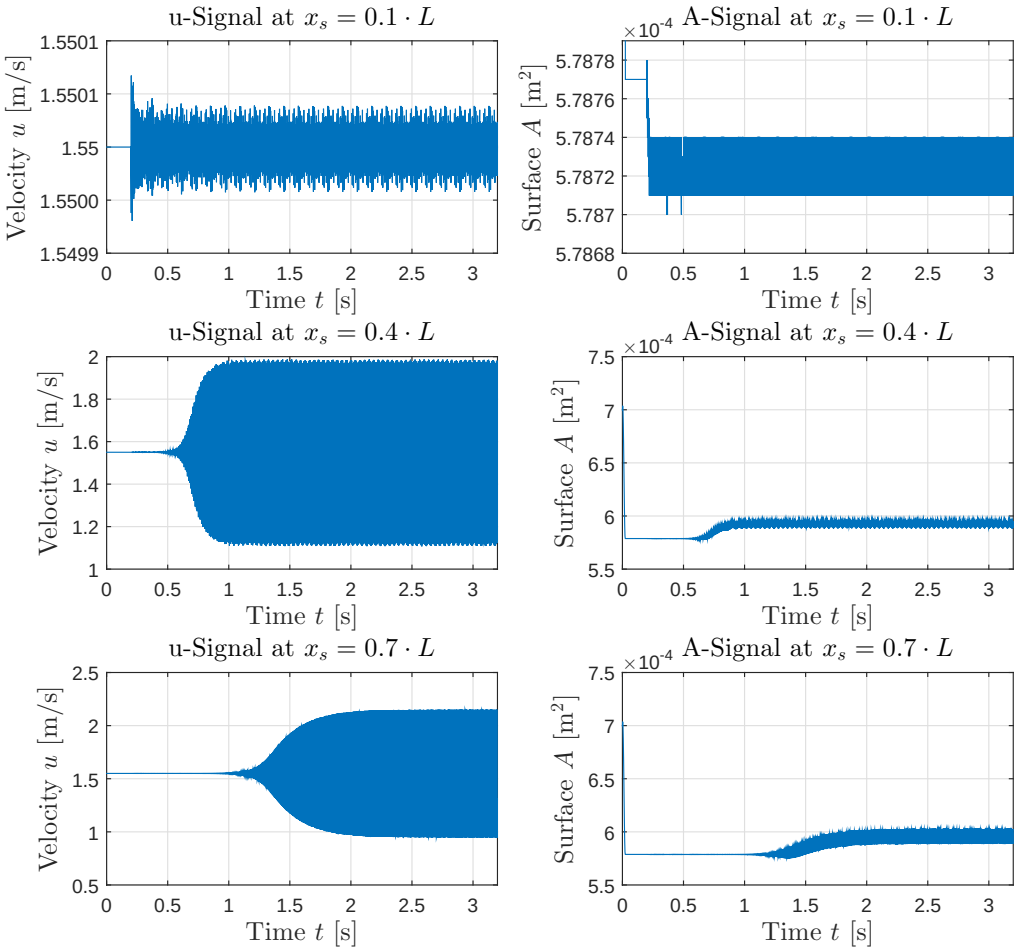

Figure 5.7: Velocity and flame surface signals of three examples plotted over time.

it has not stabilized at the moment. That is the reason why no limit cycle evolves. The low frequency of $f = 26.77$ Hz is also shown in the flame surface FFT. In the velocity signal there is no such low frequency. The only detected frequency in the velocity signal is $f = 189.3$ Hz. This frequency also appears in the FFT of the flame surface signal. Also the higher harmonics of this frequency oscillate in the surface signal. In the 3D phase portrait the oscillation seems to be a thick line. This happens because the cycle which is normally shown in this type of plots is elongated to a line and the single cycles are not even due to numerical and interpolation errors. The velocity-area-portrait demonstrates again the stabilizing of the oscillation. First the surface is much too large and is decreased in the default case with a fixed velocity value. Then it starts to oscillate and evolves to a stable oscillation.

The last example which is analysed is the system with $x_s = 0.7 \cdot L$. Here the velocity signal is sinusoidal again but now also the flame surface signal is much smoother than in the case

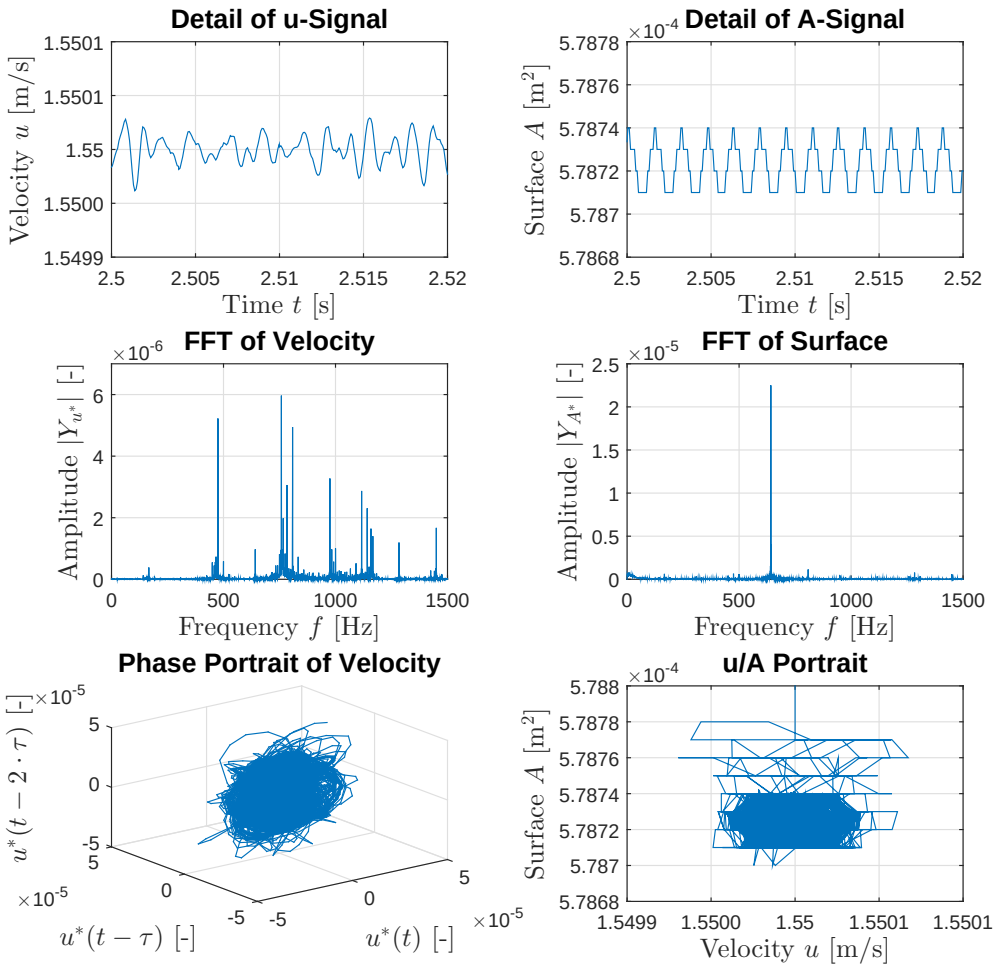

Figure 5.8: Example for $x_s/L = 10\%$.

before. In the FFT plots the dominant frequency is shown as $f = 137.3\,\text{Hz}$. That is the same value as for the dominant flame surface frequency. Here the higher harmonics also appear as multiples of the dominant frequency. Now the 3D phase portrait demonstrates a closed circular line. So this can be assumed as a limit cycle. In the velocity-area-portrait the stabilization of the oscillation is shown again as described in the cases before. It can be seen that the flame surface shift here again. The mean flame surface increases with an increasing velocity amplitude.

Now the three examples were plotted in a 2D phase portrait of the velocity which are in figure 5.11. The plots are similar to the 3D phase portrait plots but there is no direction for $u(t-2\cdot\tau)$. Instead the intersection of the 3D plot with the zero level is shown. If this intersections do not spread too much or are not evenly distributed over a range, it indicates a limit

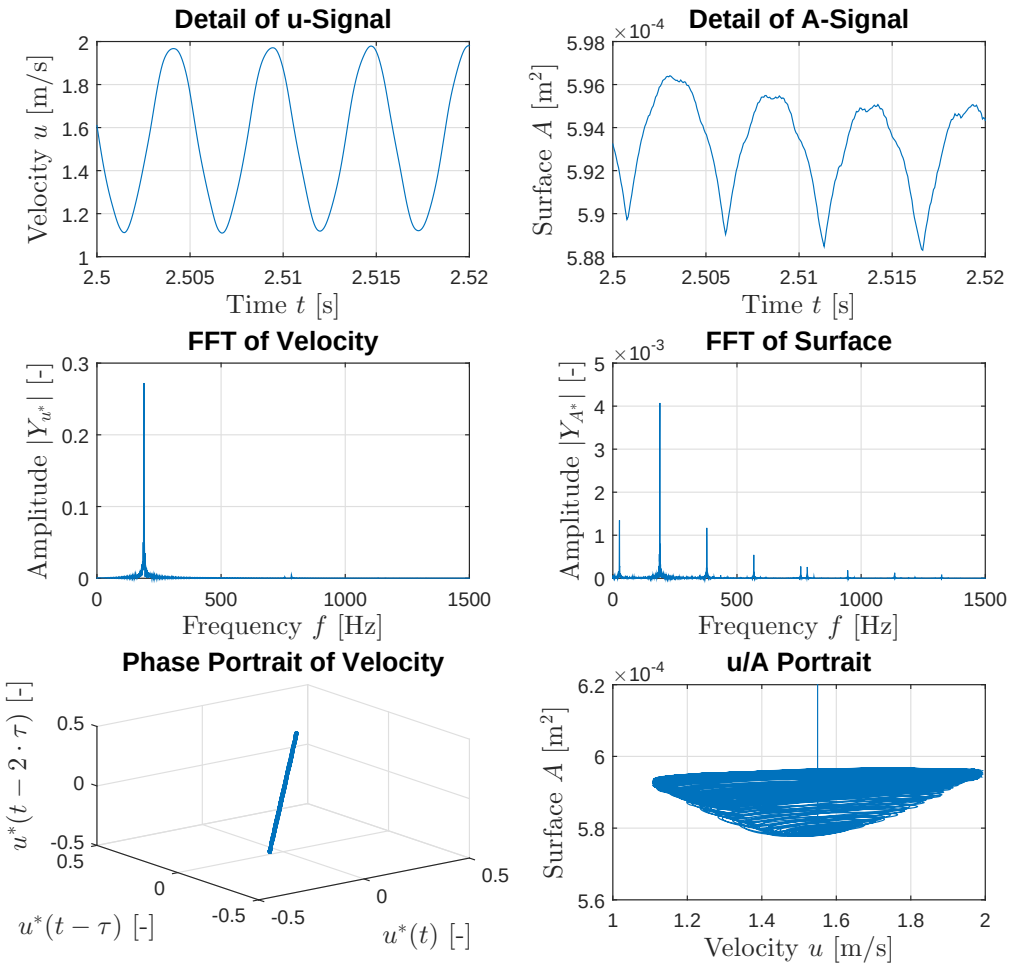

Figure 5.9: Example for $x_s/L = 40\%$.

cycle. For the first described example the behaviour is very chaotic which leads to the assumption that it is not a limit cycle. This can be seen in the first plot. The intersections are scattered and the distribution seems random. So it is not a limit cycle.

The second case is the system with the flame position $x_s = 0.4 \cdot L$. Here the intersections are also distributed but it seems that the field elongates. In this case it is hard to tell if it is a limit cycle behaviour or not. In the plot it seems that it is not a limit cycle but the scattering is caused by numerical issues and interpolation errors. It is possible that with a finer mesh in the Level-Set solver the results get more accurate and better defined intersection points appear.

The last case now shows a limit cycle. Here two intersection areas are shown which are elongated. The single intersections are scattered like in the cases before. In this case it is obvious that this scattering is caused by the interpolation.

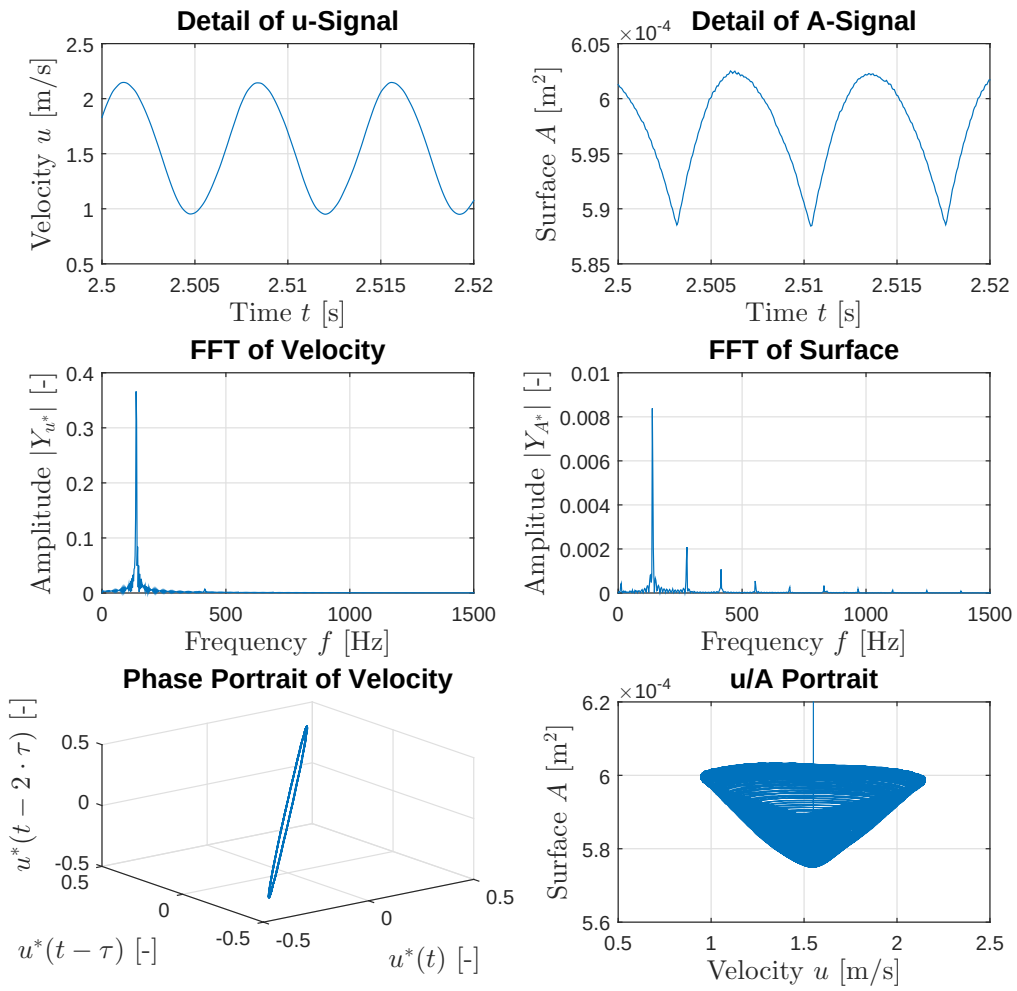

Figure 5.10: Example for $x_s/L = 70\%$.

5.4.2 Bifurcation Results

Next the results of the single simulations were merged to do a bifurcation analysis. The plot in figure 5.12 shows the results from the FFT analysis for every step of x_s. Also the predicted eigenfrequencies are plotted for the linear acoustic system with and without a flame. Until $x_s = 0.2 \cdot L$ the system is stable. Then the system starts to oscillate with a frequency of $f = 456.5\,\text{Hz}$. This frequency is almost the second eigenmode of the acoustic system without flame. Now by increasing the x_s value, the dominant frequency drops to the first eigenmode of the acoustic system. The system keeps these characteristics until $x_s = 0.6 \cdot L$. Here the flame stabilized and the oscillation disappears but at the next step it starts to oscillate again with the first acoustic mode. At $x_s = 0.7 \cdot L$ the largest amplitude after the stable point was calculated.

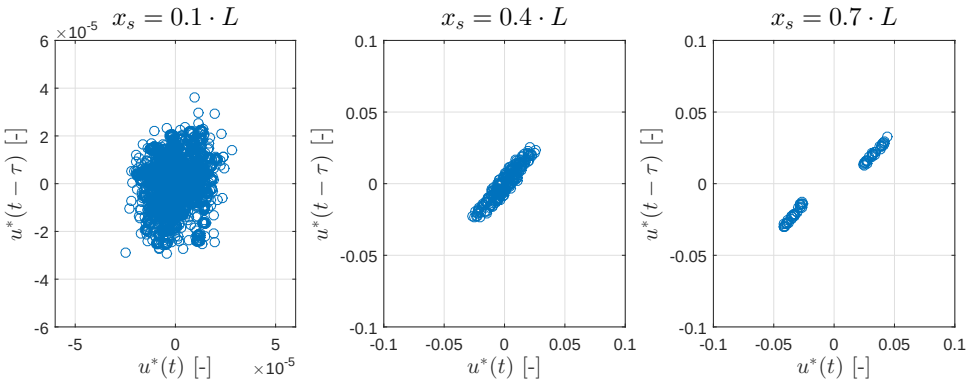

Figure 5.11: Intersection plots of the phase portraits of three examples.

At $x_s = 0.8 \cdot L$ the dominant frequency jumps up to the second eigenmode again at a frequency of $f = 367.5$ Hz. By increasing x_s again the oscillation stops and the system gets stable again.

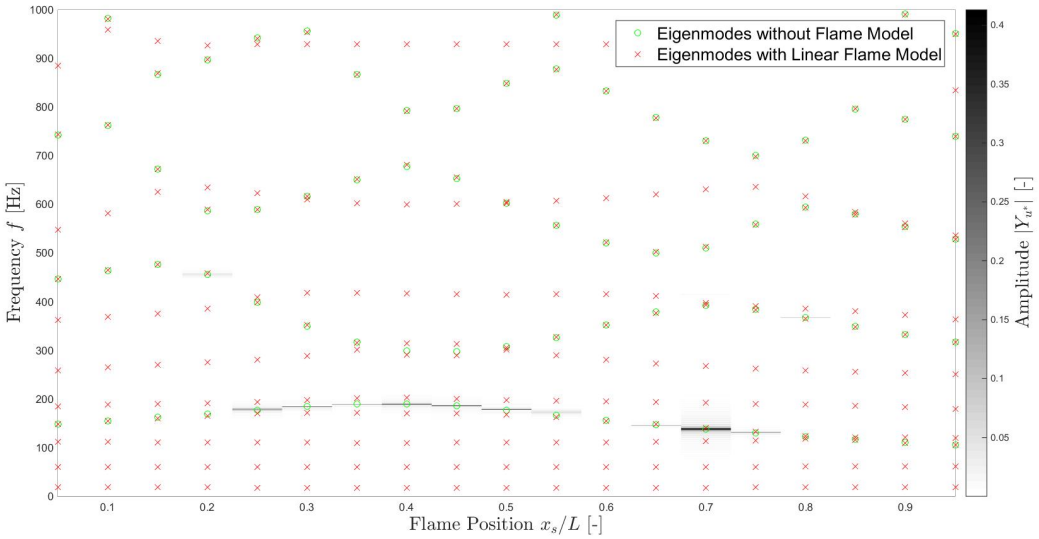

Figure 5.12: Bifurcation analysis of the velocity signal FFT results.

The FFT bifurcation plot of the flame surface in figure 5.13 shows similar results as the bifurcation plot of the velocity. The main difference is that the FFT bifurcation plot of the surface also shows the higher harmonics.

The results are similar to the results gained by Orchini et al. (2015). In this publication also at $x_s = 0.6 \cdot L$ the system is stable and at the ends also no oscillations occur. The amplitudes of the velocity are lower than in the data gained with GFlame. It is possible that this depends on the curvature influence. A model which considers the curvature is more damped than the simulation without it. This can cause a lower flame surface amplitude and also a lower velocity amplitude. In the publication also more different oscillation types appear. This can be caused

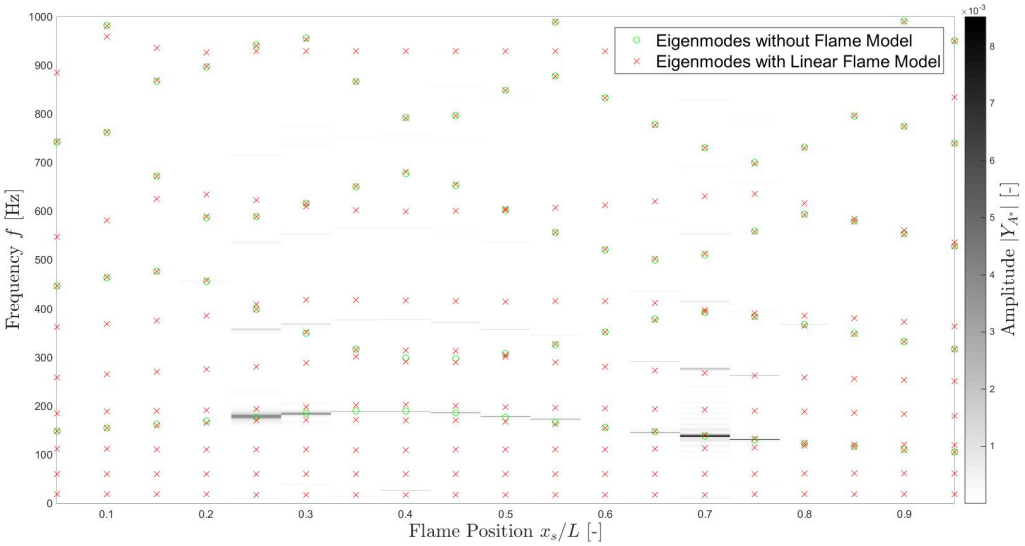

Figure 5.13: Bifurcation analysis of the flame surface signal FFT results.

by the different velocity model. A convective incompressible velocity model leads to pinch off and curvature effects which hardly appear with a convective velocity model. These effects are important for the oscillation behaviour.

The plot in figure 5.13 shows the bifurcation of the normed velocity amplitude compared to the dominant frequency of the velocity. Here the trend of the velocity signal can much better be seen. The amplitude starts to increase $x_s = 0.2 \cdot L$. At $x_s = 0.6 \cdot L$ the system gets stable and then the velocity amplitude increases again. At large amplitudes the frequency is almost stable but if the velocity amplitude is 0 the frequency shifts to a higher value. These oscillations are caused by numerical issues.

The surface amplitude bifurcation plot in figure 5.15 is pretty much the same as for the velocity signal. One effect which can be seen here is the saturation of the non-linear flame element. At higher velocity amplitudes the flame surface amplitude does not increase as strong as the velocity. This is caused by the non-linearity. Another effect can be seen in the dominant frequency. At both ends of the system the amplitudes are 0 and the frequencies are at higher values than for an unstable condition. The dominant velocity frequency here is much higher than the dominant frequency of the surface signal. This is caused by the low-pass properties of the flame element.

A property of the flame surface is that the mean value of the surface signal shifts upwards during an oscillating simulation. In figure 5.16 this shift can be seen. Overlain the amplitude of the surface signal is plotted. It can be seen that the mean surface shift depends on the amplitude of the surface signal. Also the frequency has an influence but it is much less than the amplitude. This shift can be explained by equation (5.2).

$$S_{rot} = 2 \cdot \pi \cdot r_{curve} \cdot L_{curve} \tag{5.2}$$

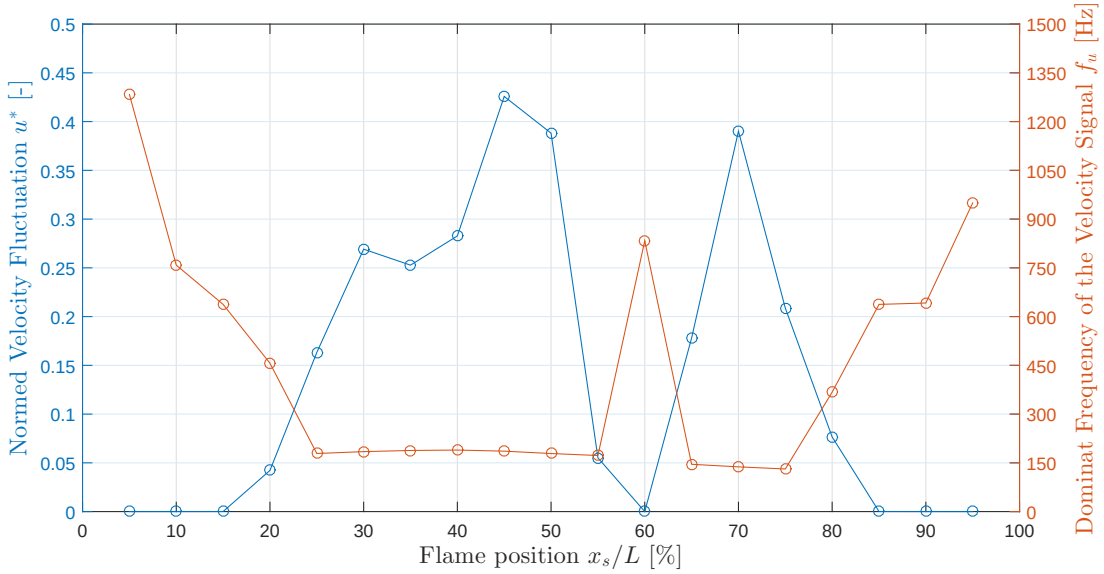

Figure 5.14: Bifurcation of the maximum velocity amplitude and the dominant velocity frequency.

This equation denotes the first rule of Guldin (see e.g. Bronštejn et al. (2013)) which can be used to calculate the curved surface area of an axially symmetrical body like the flame surface. The needed values are the distance of the center of gravity of the curve to the symmetry line r_{curve} and the length of the curve L_{curve}. If the flame is wrinkled with a high frequency the value L_{curve} increases with the velocity perturbation amplitude. On the other hand the distance value r_{curve} does not change much, so the flame surface must increase.

The last bifurcation analysis was done with the delay time until the maximum amplitude of the velocity signal and the amplitude of the flame surface signal is reached. Here the trend can be seen that the delay time is depending on the amplitude of the signal. A higher maximum amplitude needs a longer delay time. Here also the damping characteristics of the flame can be seen. In general the flame surface signal stabilizes first.

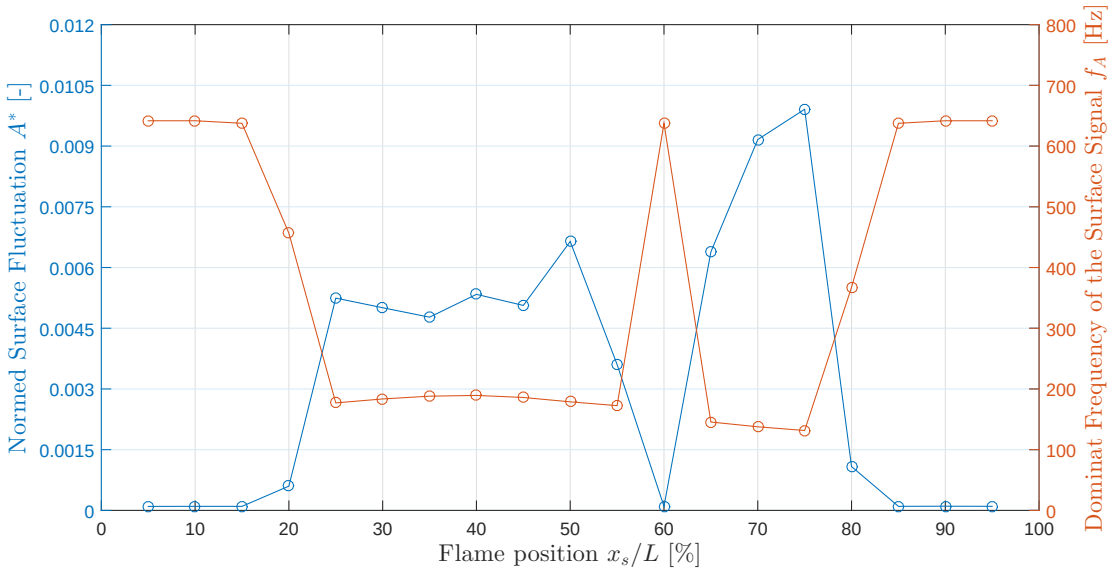

Figure 5.15: Bifurcation of the maximum flame surface amplitude and the dominant flame surface frequency.

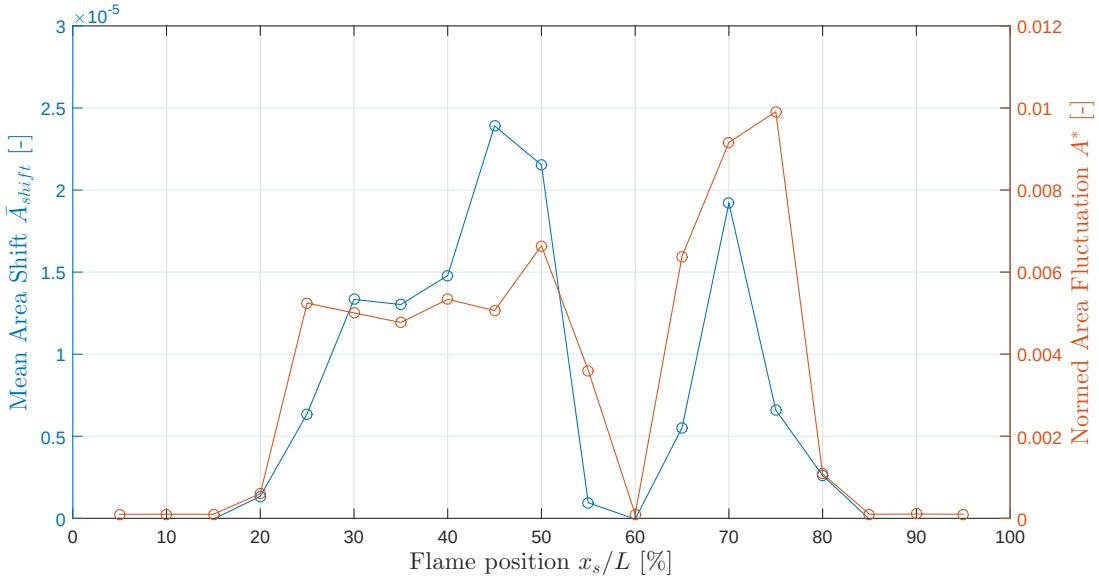

Figure 5.16: Bifurcation results of the mean flame surface shift.

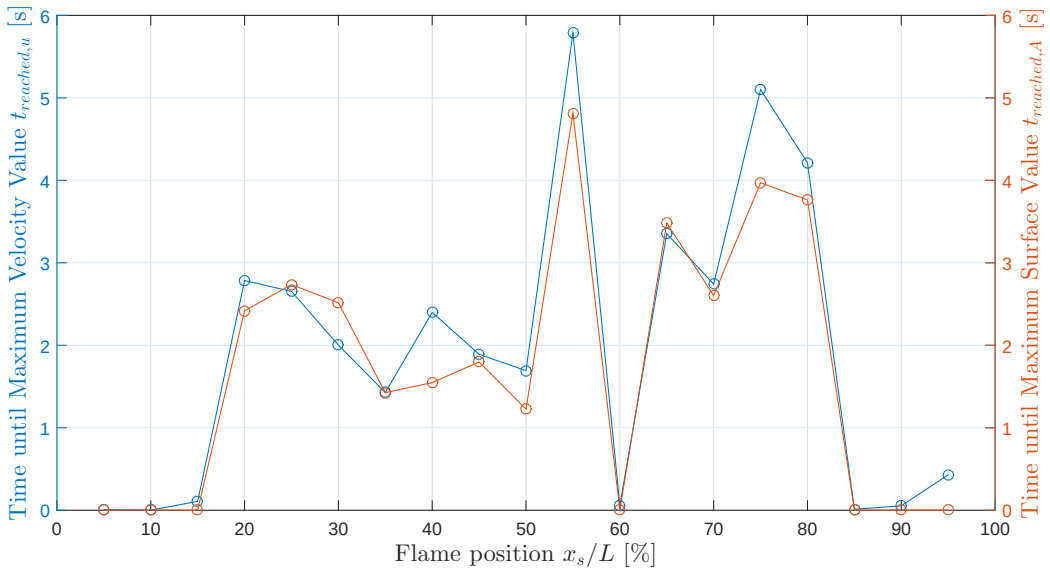

Figure 5.17: Bifurcation results for the time delay until the maximum amplitudes are reached.

6 Coupled Simulation with a Slit Flame

The last system which was considered is a thermoacoustic system described by Kornilov et al. (2009). In this publication the author did several experiments by changing different parameters of the system and tried to model the behaviour in theory. Limit cycle oscillations were not considered there. Jaensch et al. (2015) used the system to generate limit cycle behaviour. These results were gained with CFD simulations. In this chapter the rebuild of this system is described with the Level-Set solver.

6.1 Setup Description

The burner which was used in Kornilov et al. (2009) and Jaensch et al. (2015) is shown in figure 6.1. It is a burner which combusts methane and air. The acoustics are characterised by the plenum length x_s. The flames are slit flames which are positioned side by side. In order to get a computable system for GFlame, just one of the flames is considered. This was also done by Jaensch et al. (2015).

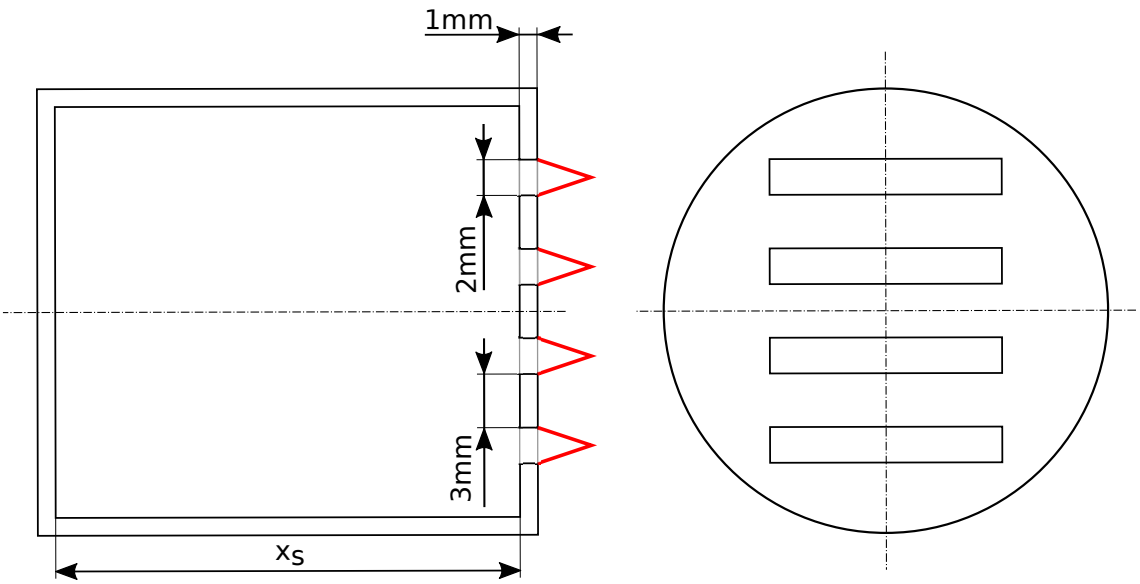

Figure 6.1: Kornilov burner

The acoustic system in Jaensch et al. (2015) was generated with taX and the same acoustic system was used in this thesis. The flame simulation was changed from a CFD simulation to the Level-Set solver.

6.2 Acoustic Setup

The acoustic setup was done in taX and is shown in figure 6.2. The system shows the plenum length which can be varied with a closed end boundary on the left side. Then the reference element for the reference velocity is positioned. Next the area jump for the flame notch is positioned. After the next area jump, which is basically the outlet of the notch, a short duct element is attached. It defines the flame lift-off. Then a non-reflecting boundary closes the system on the right side. The system is not optimized for an import to GFlame. The reason therefore is that the system was used for the CFD simulations in Jaensch et al. (2015). In order to get better comparable results the system was not changed much. The only modification was done for the cross area values which were doubled. This was done because GFlame does not use the symmetry of the acoustic system as the CFD simulation did. So these values had to be doubled.

Table 6.1: Parameters of the acoustic network model.

Name	Value
Plenum height	$H_{\text{plenum}} = 5\,\text{mm}$
Slit height	$H_{\text{slit}} = 2\,\text{mm}$
Slit length	$L_{\text{slit}} = 1\,\text{mm}$
Lift off length	$L_{\text{liftoff}} = 2.6\,\text{mm}$
Left boundary condition	$r_1 = 1$
Right boundary condition	$r_2 = 0$
Mean inlet velocity	$\bar{u}_{\text{in}} = 0.4\,\text{m/s}$
Inlet temperature	$T_{\text{in}} = 293\,\text{K}$

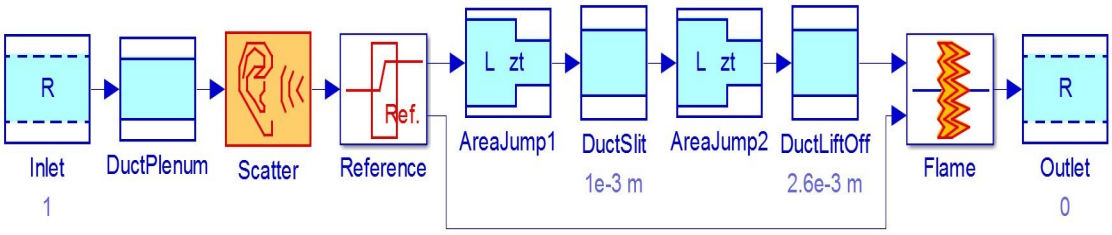

Figure 6.2: Acoustic system designed in taX.

The main parameters which were used in taX are listed in table 6.1. Note that the system is used for Cartesian coordinates which means that the areas are rectangular. The height of each element is equal to its area due to the fact that the system has a standard depth of 1 m.

Now the simulation was done for x_s values between 20 mm and 320 mm with a step of 20 mm. The system with $x_s = 0\,\text{mm}$ was excluded because there are no meaningful results expected. The boundary of $x_s = 320\,\text{mm}$ was set because in the non-linear simulation with GFlame the oscillations were so strong that the flame surface moves out of the numerical

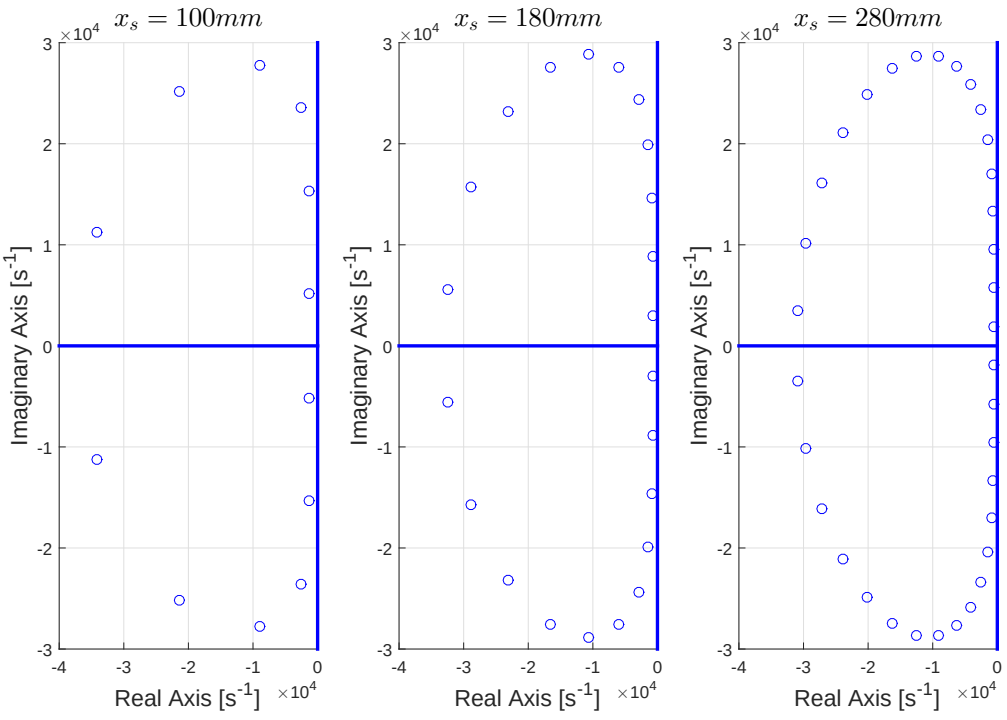

Figure 6.3: Eigenvalues of the acoustic system without flame.

mesh. In figure 6.3 the eigenvalues of three acoustic systems with deactivated flame element are shown.

They were chosen because they show different oscillation types in the non-linear simulation which are discussed in chapter 6.4. First of all one can see that the number of eigenvalues increases with the plenum length. This is caused by the discretization of the plenum tube. The discretization does not change, so a shorter tube has less eigenvalues. The more important fact is that all eigenvalues have a negative real part. That is important for the stability of the system.

6.3 Flame Setup

The non-linear flame model which was used in the Level-Set solver is now a slit flame type. This means that the transfer behaviour differs compared to a conical flame. For the combustion, a mixture of methane and air was used. The main flame properties which were used are listed in table 6.2.

The mean flow velocity differs from the inlet velocity because the slit height is smaller than the plenum height. With the continuity equation one can compute the mean velocity at the reference point. As described in chapter 5, first the flame was put into a default case. This was done by simulating the flame for 0.2 s without any perturbations. During this time the flame

Table 6.2: Parameters of the flame model.

Name	Value
Flame height	$h_f = 1\,\text{mm}$
Equivalence ratio	$\Phi = 0.8$
Mean flow velocity	$\bar{u} = 1\,\text{m/s}$

gets into a conical shape. Then the coupled simulation was resumed and the system can start to oscillate.

6.4 Simulation Results

The non-linear simulation was done for 16 different plenum lengths. The gained results were first discussed for three examples in detail which represent different behaviours. Then all data was merged to several bifurcation plots to analyse the system in dependency of the plenum length.

6.4.1 Results for Specific Flame Positions

First the raw velocity and flame surface signals were observed. The three examples which are considered have a plenum length of $x_s = 100\,\text{mm}$, $x_s = 180\,\text{mm}$ and $x_s = 280\,\text{mm}$. In figure 6.4 the signals can be seen.

The graphs of the system with a plenum length of $x_s = 100\,\text{mm}$ show the raw signals of a chaotic oscillation. The signals do not seem smooth and are very uneven. The second example with a plenum length of $x_s = 180\,\text{mm}$ generated much more smooth signals. This oscillation is, as later described, a limit cycle. The last example shows very rough signals. This is caused by the limits of the Level-Set solver. The flame surface leaves the computational grid. Then due to a reinitialisation of the G-Field routine, the flame surface is set back to the grid. This causes the peaks in the signals.

The first results which are analysed in detail are gained with a plenum length of $x_s = 100\,\text{mm}$. They are shown in figure 6.5. It can be seen that the velocity signal is an almost periodic signal but it is slightly disturbed. This can also be seen in the flame surface signal. Here the maximum amplitudes differ for each cycle. The saw tooth form of the signal is typical for all oscillating results gained with this thermoacoustic system. The dominant frequency calculated with the FFT is 695.5 Hz. This frequency is identical for the velocity and the flame surface signal. As for the conical flame the surface signal also includes the higher harmonics of the dominant frequency. Also the velocity signal shows the higher harmonics which was not the case in chapter 5. Other frequencies in both signals disturb the oscillation. These are no higher harmonics but the frequencies are the same in both signals. The phase portrait shows a very chaotic oscillation. The most unusual part is the cube shaped part of the phase portrait plot. It might be that here a numerical limit is reached which leads to this shape but it is very unlikely because the amplitudes are not that large. In the velocity-area portrait the oscillation

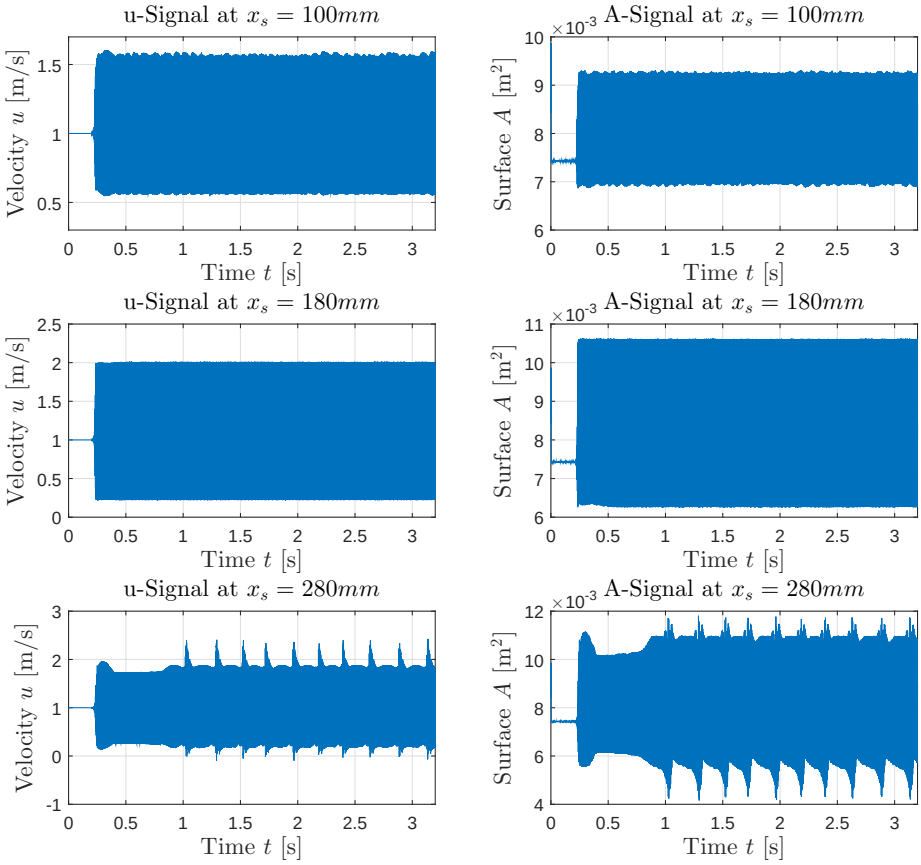

Figure 6.4: Velocity and flame surface signals of three examples.

seems more even than in the phase portrait.

The next example system has a plenum length of $x_s = 180$ mm. The results for this thermoacoustic system are depicted in figure 6.6. Now the velocity signal is more regular than in the example before. The velocity signal looks as a square wave signal which is typical for all thermoacoustic systems in this chapter. The flame surface signal is as before a saw tooth signal. Here at the maximum amplitudes it can be seen, that the first higher harmonic of the dominant frequency has a strong influence on the signal.

The dominant frequency is $f = 418.3$ Hz which can be seen in both FFT analysis. Also the higher harmonics are present in both signals. The flame surface signal is much more influenced as usual by the higher harmonics. As in the example before other frequencies are also present and disturb the signal. The phase portrait plot shows a regular shaped repeating graph which leads to the assumption that it is a limit cycle. As in the chapter 5 it is difficult to tell whether it is a limit cycle or not. The scattering might be caused by numerical effects and also the interpolation of the signal has a disturbing influence. The velocity-area portrait also

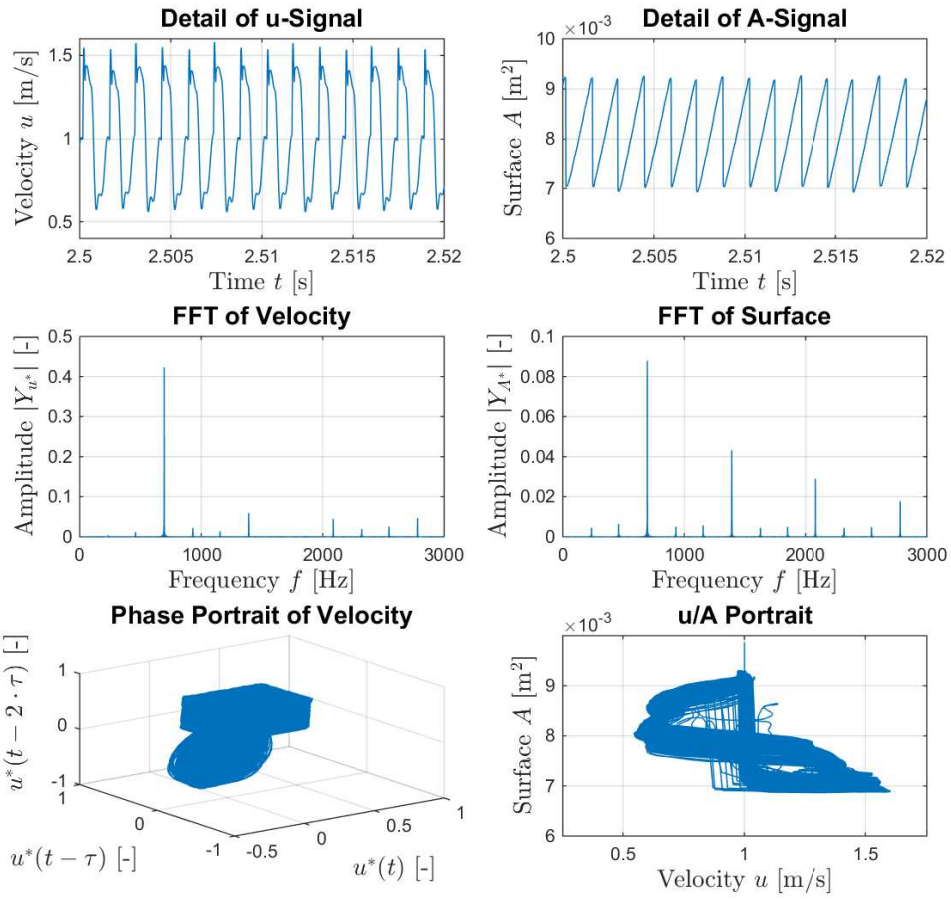

Figure 6.5: Example with a plenum length of 100 mm.

shows a very even repeating signal. The shape of this graph is comparable to the velocity-area portrait of the example before but here the graph scatters less than before.

The last example has a plenum length of x_s = 280 mm and the results are shown in figure 6.7. As described before this case is almost the limit of the Level-Set solver. The velocity amplitudes are so large that the flame surface moves out of the computational grid but due to reinitialisation routines the flame is set back to the grid. In this case it is possible to gain results but if the amplitudes are a little bit larger the simulation will not work anymore. Furthermore the results are not accurate anymore caused by errors in the flame surface calculation when the flame moves out of the grid.

Now the velocity signal looks different from the previous cases. This is caused by a lower frequency as the dominant frequency which grows and influences the signal. This behaviour can also be seen in the flame surface signal. Here it is obvious that two different frequencies act overlain. The shape of this signal stays in a saw tooth shape as for the examples before.

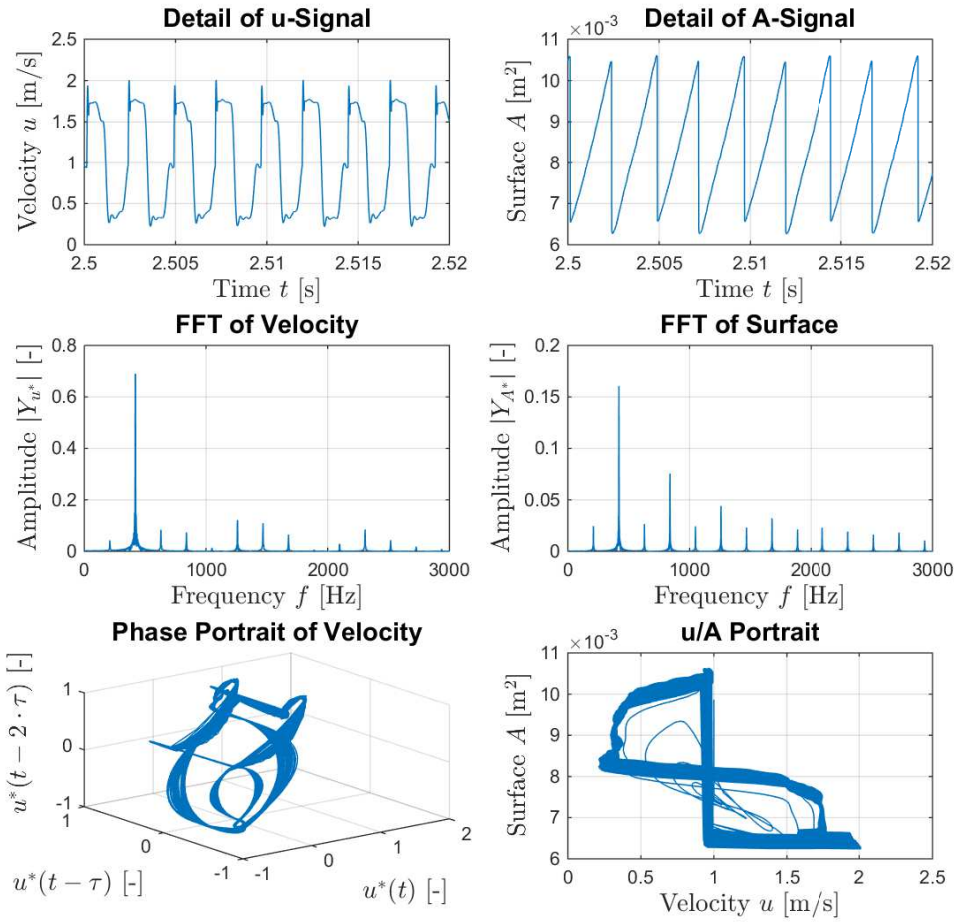

Figure 6.6: Example with a plenum length of 180 mm.

In the FFT analysis of the velocity signal, the dominant acoustic frequency can be identified as $f = 374.5$ Hz. A lower frequency $f = 185.1$ Hz is growing and its amplitude has nearly reached the amplitude of the main frequency. It is very likely that this is a so-called 'intrinsic thermoacoustic instability' (see e.g. Emmert et al. (2015)). In Jaensch et al. (2015) this also happens at a similar plenum length. In the flame surface FFT plot, the amplitude of the smaller frequency is already larger than for the acoustic frequency. The phase portrait and the velocity-area portrait are very chaotic which is caused by the numerical problems at such high velocity amplitudes.

In order to analyse the phase portraits furthermore an intersection plot was done for each example as in chapter 5. Here it can be seen that the example with the smallest plenum length has a very chaotic behaviour. The intersections scatter strongly and a limit cycle cannot be expected. The system with a plenum length of $x_s = 180$ mm has four defined intersection regions. Two of them are well defined, one is elongated and one scatters stronger than the oth-

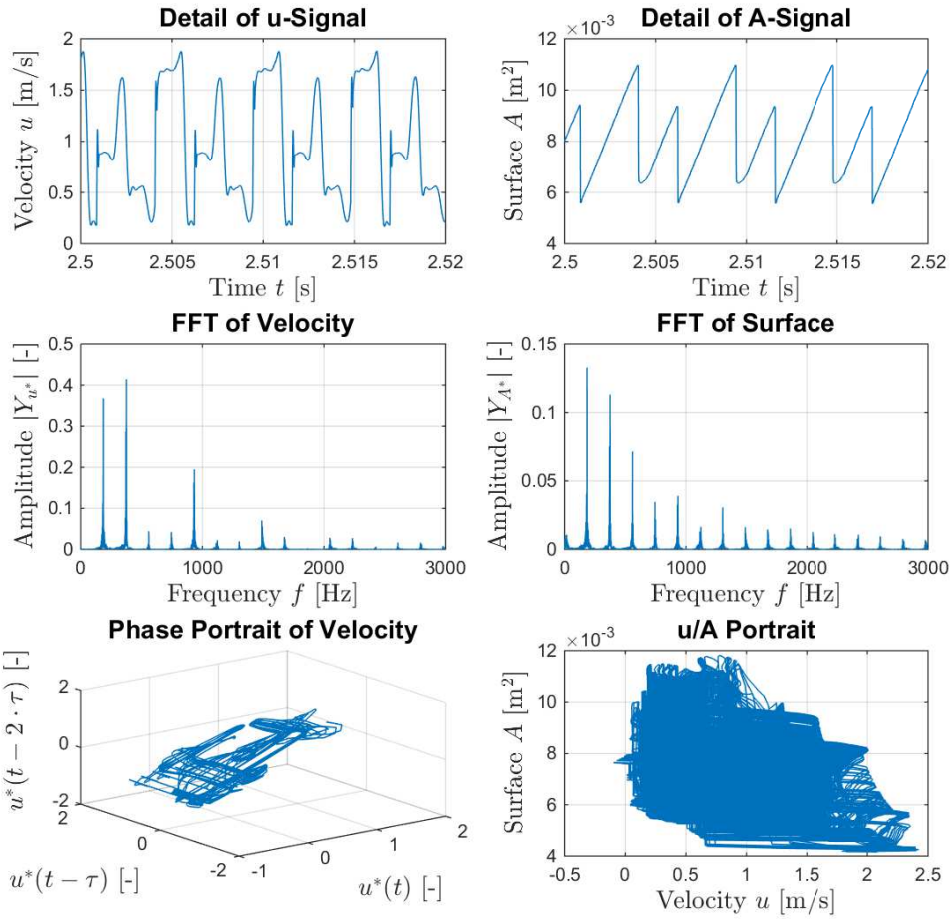

Figure 6.7: Example with a plenum length of 280 mm.

ers. As described before it is possible that these scatter effects are caused by numerical issues. The system with the largest plenum length scatters much stronger than the system before but certain intersection regions are defined. Compared to the 3D phase portrait in figure 6.7 the system seems less chaotic.

6.4.2 Bifurcation Results

As for the thermoacoustic system with a conical flame, a bifurcation analysis was done for this system. First the FFT results from the velocity signals were plotted in dependency of the plenum length. Figure 6.9 shows the results from the non-linear simulation and overlain plotted the eigenfrequencies without a linear flame model. At small plenum lengths the system does not oscillate. The first oscillation can be seen here at x_s = 100 mm. The system starts to oscillate at a high frequency. With an increasing plenum length the dominant frequency

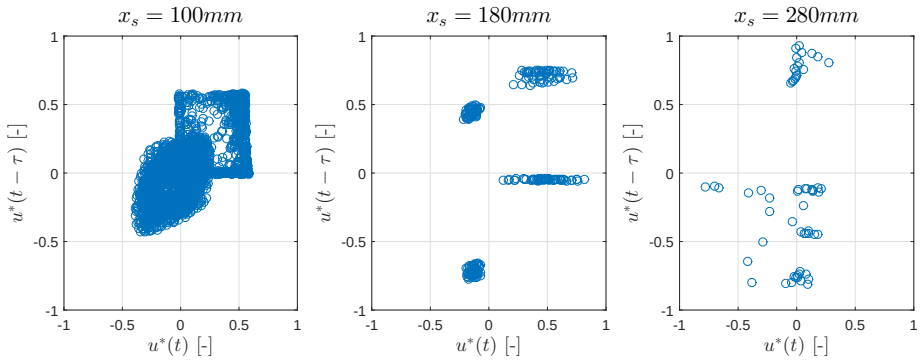

Figure 6.8: Intersection of phase portrait plots of three example systems.

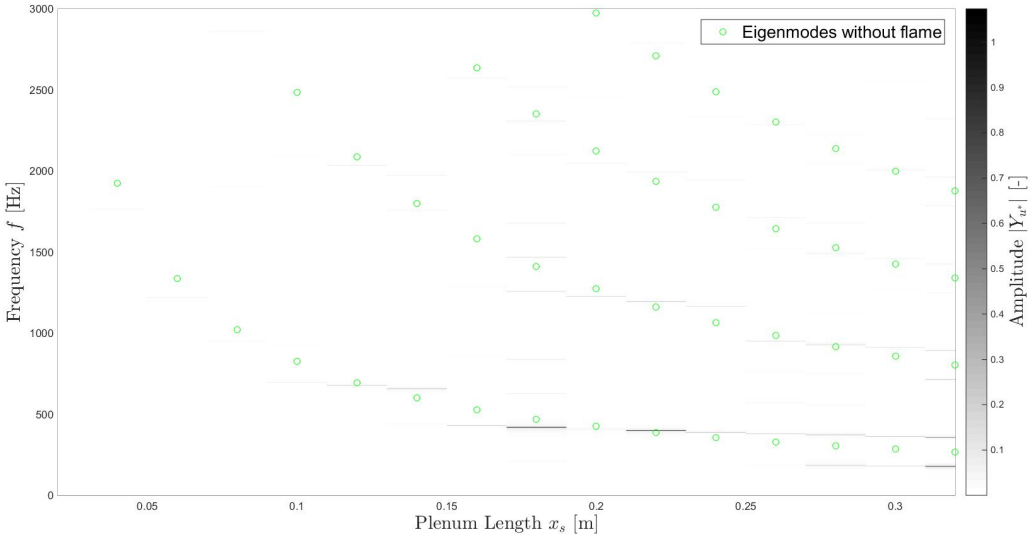

Figure 6.9: Bifurcation results of the velocity signal FFT analysis.

decreases due to the tube acoustics. At about $x_s = 150$ mm the dominant frequency drops to approximately 400 Hz and stays there until a plenum length of about $x_s = 300$ mm. Then it drops again to about 200 Hz which probably is an intrinsic frequency.

The FFT bifurcation analysis of the flame surface signals is shown in figure 6.10. It contains basically the same as the FFT bifurcation plot of the velocity signals. The higher harmonics are stronger present than in the velocity analysis.

In order to compare the change of the dominant frequency of the velocity signal with the plenum length and the maximum velocity amplitude, the bifurcation analysis in figure 6.11 was done. It can be seen that the system gets more unstable with an increasing plenum length. Also the frequency decreases with an increasing plenum length. At $x_s = 150$ mm the frequency stabilizes at about 400 Hz. At the largest plenum length the dominant frequency drops to 200 Hz. The simulation was done up to this plenum length because for larger values

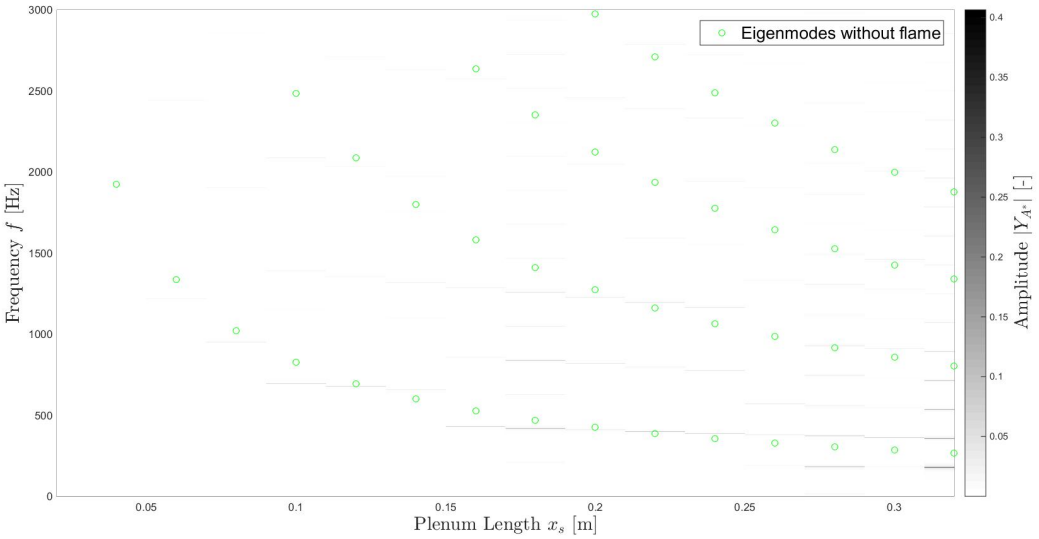

Figure 6.10: Bifurcation results of the flame surface signal FFT analysis.

the simulation did not work anymore.

The same analysis was done for the flame surface signals in figure 6.12. It shows the same trends as figure 6.11. One important fact is that the dominant frequency of the flame surface signal drops already at $x_s = 280\,\text{mm}$. At the next step it goes back to 400 Hz and then drops again. Here it can be seen that the intrinsic frequency has already a strong influence on the system before it becomes the main frequency.

As already described in chapter 5 the mean value of the flame surface signal shifts upwards during an oscillating simulation. This shift is plotted in figure 6.13. For this case with a slit flame it seems that the mean flame surface shift is almost constant and independent of the signal amplitude. Also the mean flame surface shift is very small compared to the results from chapter 5.

The last bifurcation analysis was done with the time delays until the maximum amplitude is reached in figure 6.14. Here the trend of both signals is the same. The main difference between this results and the results from figure 5.17 is that the delay times are in general smaller than for the conical flame from chapter 5. This can also be seen in figure 6.4 where the start transient is much larger than for the systems with a conical flame.

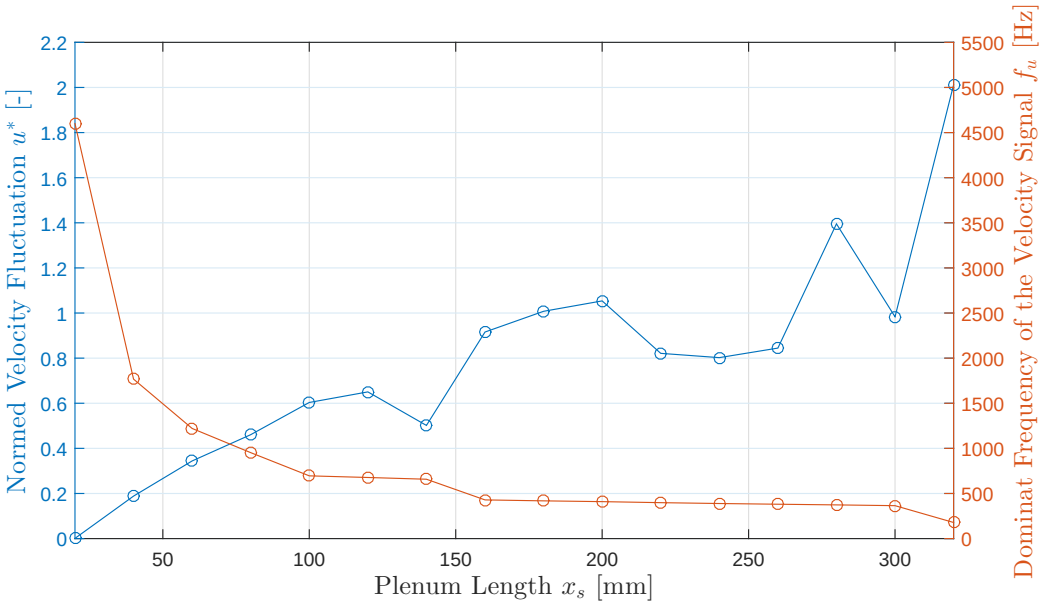

Figure 6.11: Bifurcation results of the maximum amplitude and the dominant frequency of the velocity signals.

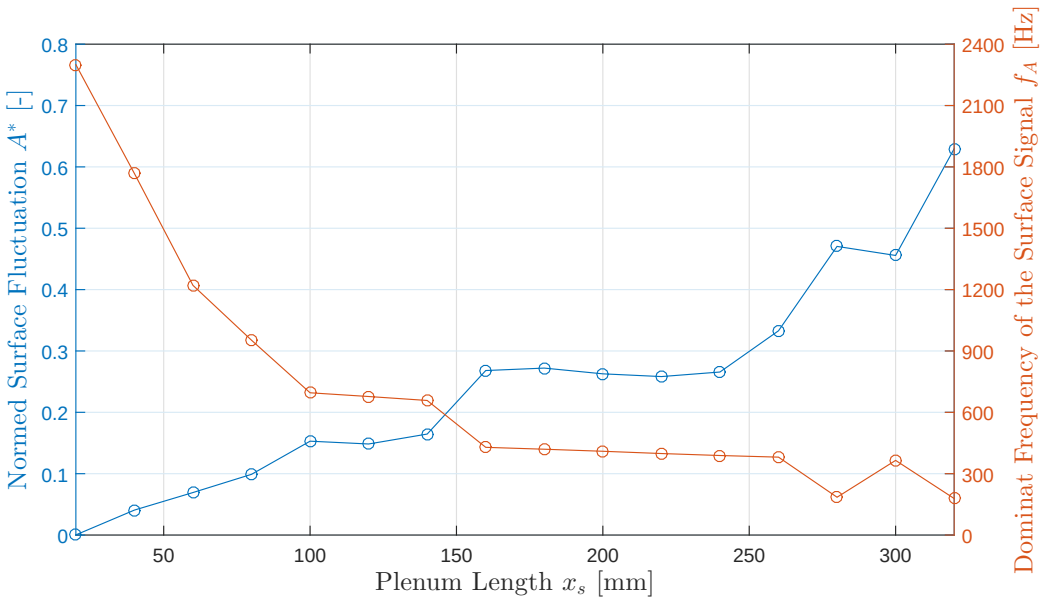

Figure 6.12: Bifurcation results of the maximum amplitude and the dominant frequency of the flame surface signals.

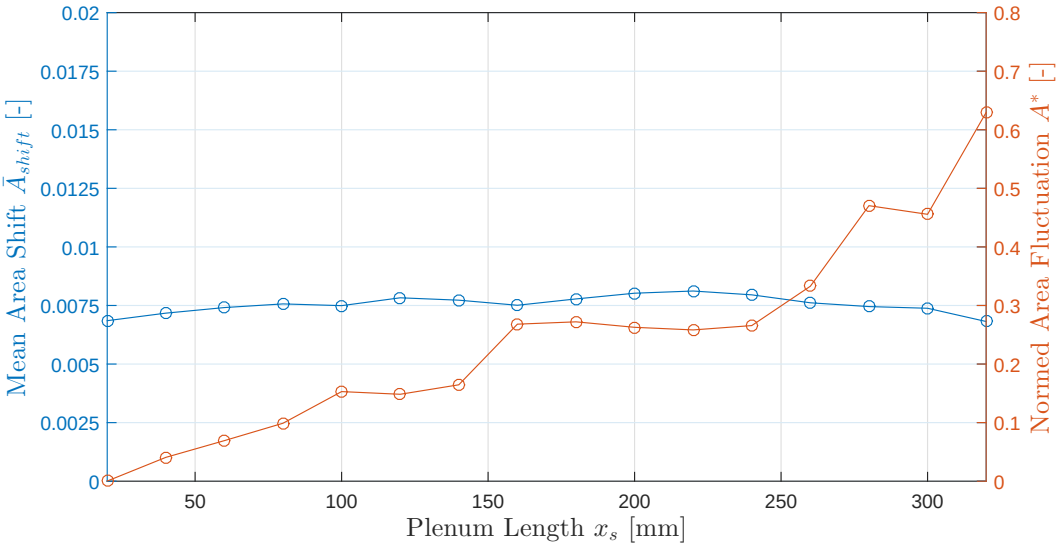

Figure 6.13: Bifurcation analysis of the main flame surface shift.

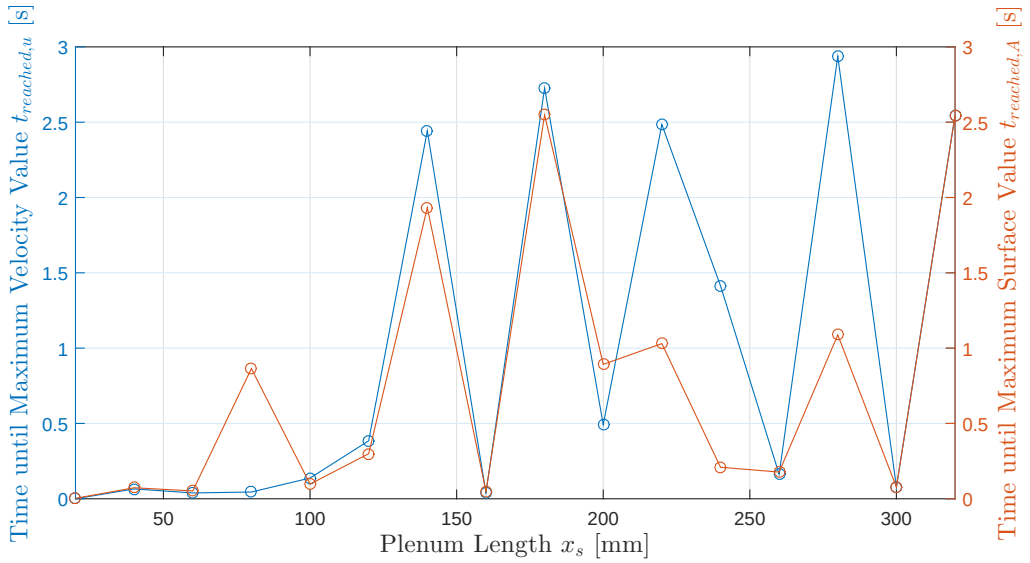

Figure 6.14: Bifurcation analysis of the start transients.

7 Conclusion

The main target of the thesis was to simulate thermoacoustic oscillations. Therefore a Level-Set solver and a low-order acoustic network model were coupled. Then two different thermoacoustic systems were considered.

First the Level-Set solver had to be verified. As reference, results from literature were taken. The first verification was a comparison between different flame contours. Here the results matched pretty well. The second graph which was used as a reference was a Flame-Describing-Function from the literature. Here the results of the gain matched in the lower frequency range. The phase behaviour differed strongly. The reason might be a numerical problem. So the simulation should be done with a finer mesh. The Sine-Sweep input signal should also be enlarged. There the numbers of periods and the number of frequencies should be increased. This may lead to better results.

After the verification, the coupling of the Level-Set solver with the acoustics program was done. This coupling was verified by recalculating an example from literature. As a first coupled system, a tube with a conical flame was considered. Inside this tube the flame position can be varied. The results were comparable and the trend of the gained data was the same. The maximum velocity amplitude was usually larger than in the reference data. This can be caused by the curvature. The results in this thesis were computed without considering the curvature. The reference data did consider the influence of the curvature. The second difference is that the oscillation type did not change that much in the recalculated results. It was also hard to tell which type exactly appeared. This can be caused by the velocity model because the convective incompressible velocity model, which was used in the reference literature, leads to other effects of the flame curvature.

The second coupled simulation was done with a burner where also results from literature were used to compare the results. In this system the plenum length was varied and the flame was a slit type. Here the trend of the results was also the same. The dominant frequency of the velocity signal was nearly the same and also the change of this frequency caused by an intrinsic frequency was reproduced. This change was at a higher plenum length as expected. It can be caused by the absence of any acoustic damping. The maximum amplitudes were also different which may be caused, as already mentioned for the first coupled system, by the curvature.

In order to conclude the results one might say that the main targets were reached. The thermoacoustic systems were recalculated and the trend of the data was as expected similar to the ones form literature. The simulations now can be improved by changing the velocity model and using the curvature influence. Also the computational grid should be refined. So the results might match even better with the reference data.

Bibliography

Bronštejn, I. N., Mühlig, H., Musiol, G., and Semendjaev, K. A. (2013). *Taschenbuch der Mathematik*. Europa-Lehrmittel Nourney, Vollmer GmbH & Co, 9. revised edition edition.

Cuquel, A., Durox, D., and Schuller, T. (2011). Theoretical and experimental determination of the flame transfer function of confined premixed conical flames. In *7th Mediterranean Combustion Symposium, Cagliari, Sardinia, Italy, September*, pages 11–15.

Dowling, A. (1997). Nonlinear self-excited oscillations of a ducted flame. *Journal of Fluid Mechanics*, 346:271–290.

Dowling, A. (1999). A kinematic model of a ducted flame. *Journal of Fluid Mechanics*, 394:51–72.

Emmert, T., Bomberg, S., Jaensch, S., and Polifke, W. (2016). Acoustic and intrinsic thermoacoustic modes of a premixed combustor. In *36th International Symposium on Combustion*, Seoul, Süd Korea. Combustion Institute.

Emmert, T., Bomberg, S., and Polifke, W. (2015). Intrinsic thermoacoustic instability of premixed flames. *Combustion and Flame*, 162(1):75–85.

Emmert, T., Jaensch, S., Sovardi, C., and Polifke, W. (2014). tax - a flexible tool for low-order duct acoustic simulation in time and frequency domain. In *DEGA Workshop Fahrzeugakustik/Strömungsakustik*, Stuttgart. DEGA.

Ferziger, J. H. and Perić, M. (2008). *Numerische Strömungsmechanik*. Springer, Berlin.

Fleifil, M., Annaswamy, A., Ghoneim, Z., and Ghoniem, A. (1996). Response of a laminar premixed flame to flow oscillations: A kinematic model and thermoacoustic instability results. *Combustion and Flame*, 106(4):487–510.

Gottlieb, S. and Shu, C.-W. (1998). Total variation diminishing runge-kutta schemes. *Mathematics of Computation*, 67(221):73–85.

Heckl, M. A. (1988). Active control of the noise from a rijke tube. *Journal of Sound and Vibration*, 124(1):117–133.

Hirsch, C. (2007). *Numerical computation of internal and external flows: Fundamentals of computational fluid dynamics*. Elsevier/Butterworth-Heinemann, Oxford and Burlington, MA, 2. Edition edition.

Jaensch, S., Merk, M., Gopalakrishnan, E., Bomberg, S., Emmert, T., Sujith, R. I., and Polifke, W. (2015). Hybrid CFD/ low order modeling of thermoacoustic limit cycles. In *Sonderforschungsbereich/Transregio 40 - Summer Program Report 2015*, TUM Garching. DFG.

Kashinath, K., Hemchandra, S., and Juniper, M. P. (2013a). Nonlinear phenomena in thermoacoustic systems with premixed flames. *Journal of Engineering for Gas Turbines and Power*, 135(6):061502.

Kashinath, K., Hemchandra, S., and Juniper, M. P. (2013b). Nonlinear thermoacoustics of ducted premixed flames: The influence of perturbation convection speed. *Combustion and Flame*, 160(12):2856–2865.

Kashinath, K., Waugh, I. C., and Juniper, M. P. (2014). Nonlinear self-excited thermoacoustic oscillations of a ducted premixed flame: Bifurcations and routes to chaos. *Journal of Fluid Mechanics*, 761:399–430.

Kopitz, J. and Polifke, W. (2008). Cfd-based application of the nyquist criterion to thermoacoustic instabilities. *Journal of Computational Physics*, 227(14):6754–6778.

Kornilov, V. N., Rook, R., ten Thije Boonkkamp, J., and de Goey, L. (2009). Experimental and numerical investigation of the acoustic response of multi-slit bunsen burners. *Combustion and Flame*, 156(10):1957–1970.

Lieuwen, T. (2003). Modeling premixed combustion-acoustic wave interactions: A review. *Journal of Propulsion and Power*, 19(5):765–781.

Lunze, J. (1996). *Regelungstechnik 1: Systemtheoretische Grundlagen, Analyse und Entwurf einschleifiger Regelungen*. Springer-Lehrbuch. Springer, Berlin, 1. edition edition.

Mitchell, I. (2008). The flexible, extensible and efficient toolbox of level set methods. *Journal of Scientific Computing*, 35(2-3):300–329.

Noiray, N., Durox, D., Schuller, T., and Candel, S. (2008). A unified framework for nonlinear combustion instability analysis based on the flame describing function. *Journal of Fluid Mechanics*, 615:139.

Orchini, A., Illingworth, S., and Juniper, M. (2015). Frequency domain and time domain analysis of thermoacoustic oscillations with wave-based acoustics. *Journal of Fluid Mechanics*, 775:387–414.

Osher, S. and Sethian, J. A. (1988). Fronts propagating with curvature-dependent speed: Algorithms based on hamilton-jacobi formulations. *Journal of Computational Physics*, 79(1):12–49.

Poinsot, T. and Veynante, D. (2005). *Theoretical and numerical combustion*. Edwards, Philadelphia, 2. edition edition.

Polifke, W. (2004). Combustion Instabilities. Internal Document, Professur für Thermofluiddynamik, TUM Garching.

Rayleigh (1878). The explanation of certain acoustical phenomena. *Nature*, 18(455):319–321.

Schuller, T., Durox, D., and Candel, S. (2003). A unified model for the prediction of laminar flame transfer functions. *Combustion and Flame*, 134(1-2):21–34.

Serna, S. and Qian, J. (2006). Fifth-order weighted power-eno schemes for hamilton-jacobi equations. *Journal of Scientific Computing*, 29(1):57–81.

Steinbacher, T. (2016). GFlame. Software, Professur für Thermofluiddynamik, TUM Garching. *steinbacher@tfd.mw.tum.de*.

Sujith, R., Juniper, M., and Schmid, P. (2016). Non-normality and nonlinearity in thermoacoustic instabilities. *International Journal of Spray and Combustion Dynamics*, 8(2):119–146.